POLITECNICO
MILANO 1863

SCUOLA DI INGEGNERIA INDUSTRIALE
E DELL'INFORMAZIONE

Coupling of the medium fidelity solver DUST with a helicopter simulator

TESI DI LAUREA MAGISTRALE IN
AERONAUTICAL ENGINEERING
INGEGNERIA AERONAUTICA

Author: **Serena Susanna Sganzerla**

Student ID: 945718
Advisor: Giuseppe Quaranta
Academic Year: 2022-23

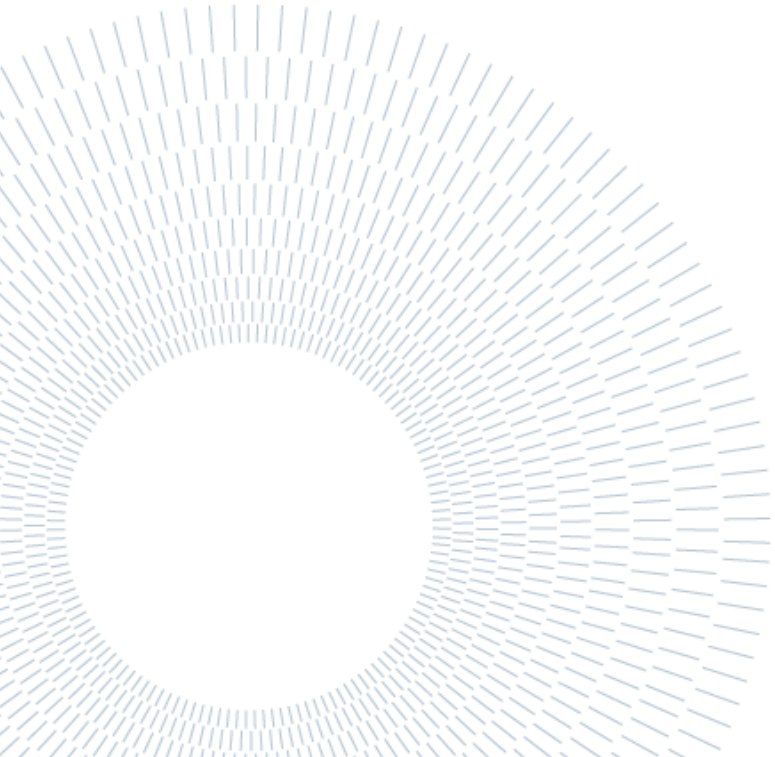

Abstract

The following document describes experimental coupling of a helicopter training simulator with a medium fidelity solver to model the rotor inflow. The scope is to develop a model based on the vortex particle method (VPM), to substitute the existing Peters-Ha model. The rotor model of the medium fidelity solver DUST has been in the first place validated in trim conditions, comparing the loads obtained with those expected from the simulator. Subsequently, a manoeuvre of interest has been reconstructed in DUST to obtain the inflow states and the loads requested to model the inflow. The new system has been identified through Levenberg-Marquardt method and introduced in the simulator in place of the old.

The compatibility of the obtained results with the expected proves the potential of the application of VPM, but also underlines how a practical implementation is currently hindered by technology limitation. The vastity of the scenarios performed in simulations and the real-time requirements are the main hurdles that would be leaped over with more powerful hardware and more efficient implementations of VPM.

Key-words: helicopter training simulator, vortex particle method, medium fidelity solver, DUST, Levenberg-Marquardt method, multiblade coordinates

Abstract in Italiano

Il seguente documento descrive l'accoppiamento sperimentale di un simulatore di addestramento per elicotteri con un risolutore di media fedeltà per modellare il flusso indotto del rotore. Lo scopo è sviluppare un modello basato sul metodo delle particelle vorticose (VPM) per sostituire l'esistente modello Peters-Ha. Il modello del rotore del risolutore di media fedeltà DUST è stato inizialmente convalidato in condizioni di assetto, confrontando i carichi ottenuti con quelli attesi dal simulatore. Successivamente, è stata ricostruita una manovra di interesse in DUST per ottenere gli stati del flusso indotto e i carichi necessari per modellarlo. Il nuovo sistema è stato identificato attraverso il metodo Levenberg-Marquardt e introdotto nel simulatore in sostituzione dell'esistente.

La compatibilità dei risultati ottenuti con quelli attesi dimostra il potenziale dell'applicazione del VPM, ma sottolinea anche come un'implementazione pratica sia attualmente ostacolata dalle limitazioni tecnologiche. La vastità degli scenari rappresentabili nelle simulazioni e il requisito di tempo reale sono le principali sfide che verranno superate con l'avvento di hardware più potenti ed implementazioni più efficienti del VPM.

Parole chiave: simulazione di addestramento per elicotteri, metodo delle particelle vorticose, risolutore di media fedeltà, DUST, metodo Levenberg-Marquardt, coordinate multipala

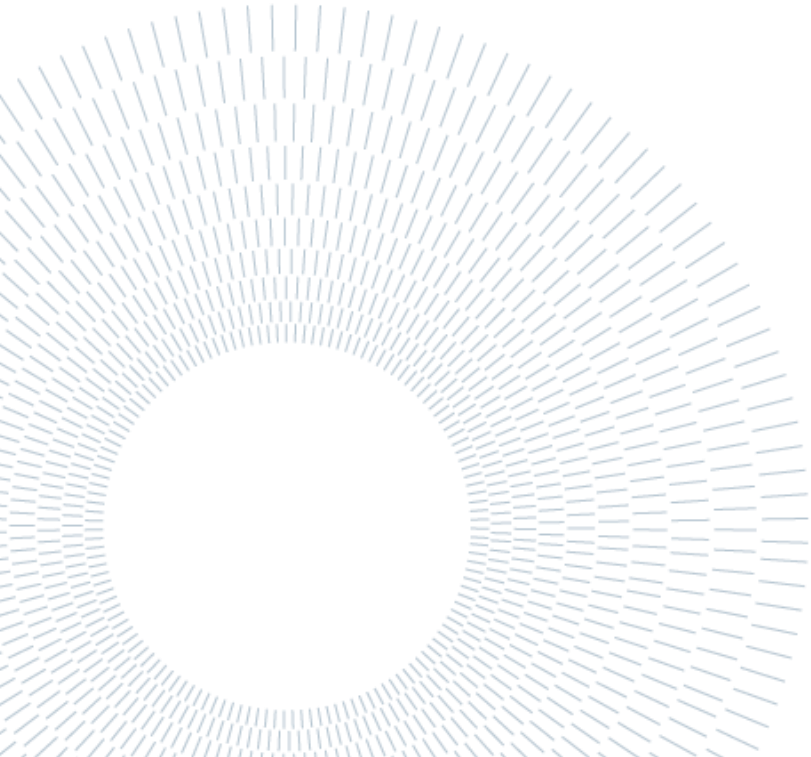

Contents

Introduction

Simulation is of main importance for both aircrafts and rotorcraft and is constantly evolving to improve the fidelity of the model while respecting the requirements imposed by regulation, particularly those concerning executional time. Models need to be simple enough to be run in real time, but also detailed enough to correctly represent the behaviour of the real aircraft. Concerning rotorcrafts, one of the fields with the most room for improvement is the aerodynamics of the rotor. Moreover, improving existing aerodynamics models is of great importance due to the growing interest of non-conventional configurations, increasingly adopted in eVTOLs. Many examples of the benefits of the exploitation of more complex models, such as those presented in [1], [2], [3] and [4] can be found in literature.

The present thesis describes the stage work I carried out at TXT e-tech S.r.l., concerning the coupling of an existing commercial simulator with a medium fidelity aerodynamics solver, in order to apply an inflow model based on the Vortex Particles Method.

In the first chapter are presented brief descriptions of the state of the art of rotorcraft simulation, of the simulator and, finally of the solver DUST.

In the second chapter is described the validation process of the model implemented on DUST with respect to that of the simulator.

In the third chapter is presented the new inflow model, how it has been obtained from DUST, how results have been processed and how it has been introduced in the simulator.

Finally, in the last chapter, are presented the results, possible improvements, and future developments.

1. State of the art

In this chapter are presented the simulator and the medium fidelity solver.

Firstly, a general insight on rotorcraft simulation is reported. Subsequently, the used commercial simulator is described, with particular focus on the modelling choices. Lastly, the medium fidelity solver DUST is presented.

1.1. Rotorcraft simulation

Rotorcraft simulation is a field of the interest, particularly for pilot training, as it allows performing potentially dangerous manoeuvres while granting both fidelity and safety for all the involved personnel and the machine itself. Flight simulation training devices (FSTD) are subjected to strict regulations by international organs such as EASA [5] and are classified according to the level of fidelity with respect to the real aircraft. The lowest level is represented by Flight and Navigation Procedures Trainer (FNPT), that only represents the flight environment. A Flight Training Device (FTD) consist in an exact replica of the aircraft, including the cockpit environment, the equipment and software. The simulation software that contains the model discussed in the following pages, will be included in a Full Flight Simulator (FFS). FFS are required of the highest compliance, with a full-size replica of the aircraft and its systems, a force cueing motion system to simulate the behaviour of the helicopter and a visual system to simulate an out of flight view. All the FSTD are subject to tests to be certified, such as validation, function, and subjective tests. The performances of the model are validated through a Qualification Test Guide (QTG) a document that confronts the performances of the FSTD with those of the real aircraft and guarantees that they are within the prescribed limits and that all the requirements are met. One

of the most important requirement is that the simulation must be performed in real time. Regulations prescribe that the transport delay, namely the total processing time needed by the FTDS, from the pilot input to the complete system response, must be below 100 ms for FFS. Transport delay includes not only the time needed by the flight model, but also that of the visual system, the motion system and the instrument response and do not include the characteristic delay of the simulated aircraft. Therefore, the flight model needs to be the best compromise between accuracy and performance. Figure 1-1 shows an example of a working FFS.

The flight model in use in the FFS of interest is called a Generic Flight Model (GFM). The GFM is an approach exploited since the beginning of rotorcraft simulation to

maximise the usability of the simulator itself. [6] The GFM has a modular structure that allows to model each aspect of the aircraft separately (i.e., flight dynamic module, engine module, transmission module…), to easily modify part of the model without impacting the others. Moreover, it is highly parametrized so that most of the aspects of the aircraft of interest can be introduced in the model without modifying it. The main advantage of the GFM is that is no longer linked to a specific aircraft but can be used for all aircraft of a certain category.

In the following, the term simulator will refer mainly to the flight dynamics module of the GFM.

Figure 1-1 An FFS (credit: Lufthansa Aviation Training)

1.2. The existing simulator

In the following is briefly presented the flight dynamics module of the existing simulator, focusing on the rotor and inflow models. [7]

The simulated helicopter is a light utility twin engine, with a customizable number of blades. The model is based on an articulated rotor with a 6 degrees of freedom (DoF) dynamic (flap β and lead-lag ζ), that occurs in coincident hinges at a specified offset. To also represent bearing-less and hinge-less rotors, concentrated springs and damper are considered for both flap and lag dynamics (flap damping factor is typically left set to 0). Blade elasticity is not considered, as it would limit the configurability of the model. Blades are therefore considered rigid, with mass distributed along the span. A multiblade coordinate system has been chosen in the model. Rotation is not directly

considered, as loads are obtained averaging over the required number of blades the output of a series of overlapping rotor. Such a solution has been chosen to improve the stability of the dynamic response, at the price of losing the contribution of the blade when in a position different of that imposed. Loads are computed trough the numerical integration along each blade of the results from blade element theory. The integration field can be defined considering tip and root cut-off, to avoid 3D effects.

The blade is defined with a series of points aligned spanwise, to which are assigned the corresponding blade element properties (i.e., chord, twist, aerofoil…). The aerodynamic coefficients for drag and lift C_D and C_L are obtained from tables, while the moment coefficient C_M is always set to zero as the pitching moment contribution on the blade element is neglected. Coefficients are obtained with CFD and are tabulated according to angle of attack, aerofoil, and Mach number. Angles of attack cover a 360° range to capture reverse stall and local blade stall. To find the Mach number and the angle of attack, the velocity of the blade element $\bar{U}_b$ is needed.

$$\bar{U}_b = \bar{V}_b + \bar{V}_{in} \qquad 1.1$$

$\bar{U}_b$ is computed as in 1.1, where $\bar{V}_b$ is the local velocity of the blade element, obtained by transporting the contribution of linear and angular speed of the helicopter in the local reference frame and $\bar{V}_{in}$ is the inflow velocity. It is therefore clear that a reliable and accurate inflow model is needed.

1.2.1. Inflow model

In the simulator is implemented the Peters-Ha inflow model [8], an evolution of the Pitt-Peters model, traditionally used for the scope [9]. In this model the inflow is assumed to have the form in 1.2

$$\lambda(r, \bar{\psi}) = \lambda_0 + \lambda_s \frac{r}{R} \sin\bar{\psi} + \lambda_s \frac{r}{R} \cos\bar{\psi} \qquad 1.2$$

Where λ_0, λ_s, λ_c are the uniform, lateral and longitudinal variation. Their time history is described by the first order differential equation in 1.3

$$[M]\begin{Bmatrix}\dot{\lambda}_0\\ \dot{\lambda}_s\\ \dot{\lambda}_c\end{Bmatrix} + [L]^{-1}\begin{Bmatrix}\lambda_0\\ \lambda_s\\ \lambda_c\end{Bmatrix} = \begin{Bmatrix}C_T\\ C_l\\ C_m\end{Bmatrix} \quad 1.3$$

[M] is the apparent mass matrix, that denotes the time delay due to the wake (1.4), [L] is the inflow gain matrix (1.5), and C_T, C_l, C_m are the thrust, roll moment, and pitching moment coefficients, only considering the aerodynamic contribution.

$$[M] = \begin{bmatrix}\frac{128}{3\pi} & 0 & 0\\ 0 & \frac{16}{45\pi} & 0\\ 0 & 0 & \frac{16}{45\pi}\end{bmatrix} \quad 1.4$$

$$[L] = [\tilde{L}][V]^{-1} \quad 1.5$$

Where $[\tilde{L}]$ is a matrix depending on the wake angle χ as in 1.6, and [V] is a matrix containing the weighted down stream velocity, depending on λ_m and μ, respectively the nondimensional inflow velocity from momentum theory and the nondimensional stream velocity.

$$[\tilde{L}] = \begin{bmatrix}\frac{1}{2} & 0 & -\frac{15\pi}{64}\sqrt{\frac{1-\sin\chi}{1+\sin\chi}}\\ 0 & \frac{4}{1+\sin\chi} & 0\\ -\frac{15\pi}{64}\sqrt{\frac{1-\sin\chi}{1+\sin\chi}} & 0 & \frac{4\sin\chi}{1+\sin\chi}\end{bmatrix} \quad 1.6$$

The Peters-Ha model introduces a perturbation matrix [δL] that corrects the model considering wake angles and velocity, so that the final [L] is equal to 1.7.

$$[L] = [\tilde{L}][V]^{-1} + [\delta L] \quad 1.7$$

This wake correction is implemented in the GFM to be activated and deactivated at need.

This first harmonic, non-uniform model has been proved a solid solution to predict the on-axis response [10], moreover is optimal for the real time requirement. Nevertheless, it does not adequately represent the off-axis response, leading to the need of a massive tuning of the results, particularly during simulation of maneuvers.

An increasingly used solution is that of pairing the simulator to a medium-fidelity aerodynamics solver, through look-up tables or direct coupling, to exploit more advanced models to describe the inflow and the wake, such as vortex particles method, without recurring to time consuming method as CFD.

1.3. DUST

DUST is an open-source mid-fidelity aerodynamical solver developed at Politecnico di Milano [11]. It is developed in Fortran language, and it can simultaneously exploit different modelling techniques to solve the aerodynamics problem. In the following, its working flow and modelling techniques are briefly presented.

The code is divided in three parts, a preprocessor, a solver, and a postprocessor. The preprocessor defines the geometry of the problem, based on the user input, that can be either parametric, CAD mesh, or a mix of the two. The solver takes as input the results of the preprocessor, the reference frames with their motions and the simulation parameters imposed by the user, and gives as output the results of the computation. Those results are processed according to user's needs in the postprocessor. A more detailed explanation of the general usage of DUST would be out of the scope of this document, however a case related explanation of inputs and outputs can be found in chapter 4. A graphic representation of the workflow is in Figure 1-1.

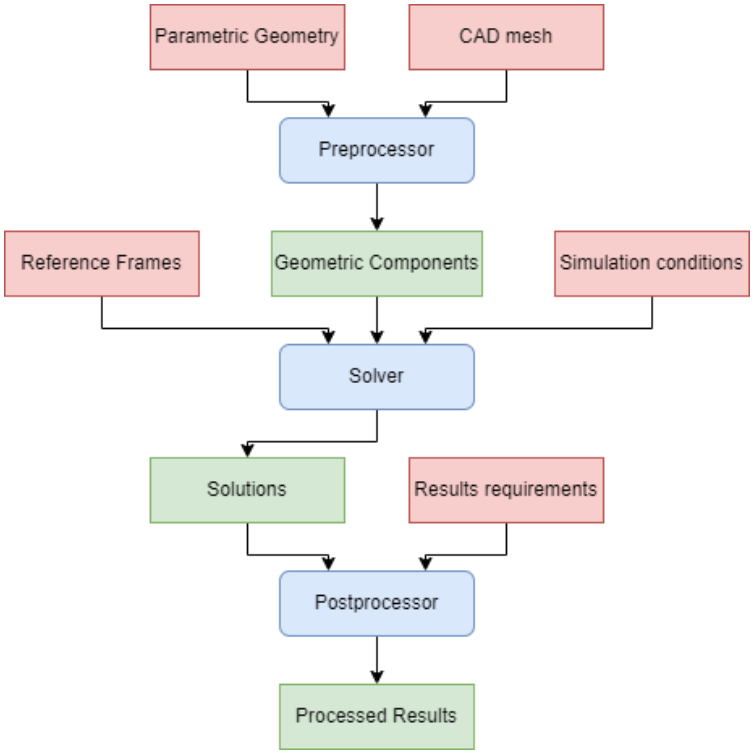

Figure 1-2 DUST workflow

The code allows only rigid components and an incompressible potential flow, even though compressibility effects can be imposed with Mach dependent aerodynamic tables. Lifting bodies can be modelled as vortex sheets (two dimensional) or lifting lines (one dimensional), while solid bodies are modelled with surface panels. Wake is shed from the trailing edge of lifting bodies, and it is modelled with vortex panels, that convert into vortex particles after a prescribed number of timesteps. The intensity of the particle is obtained integrating the contributions of the sides of the vortex panel, taking into account the asymmetries due to the presence of neighbouring elements (else the integral would result null). The main advantage of the vortex particle method is the ability to accurately describe the interaction between the wake and other elements without recurring to prescribed wake models and without incurring in instabilities due to interconnecting vortices that cross structural element.

In the following chapters is explained how the simulator and DUST have been paired, to obtain a new inflow model, based on a free wake aerodynamic analysis.

2. Validation of the DUST model

In the following chapter is presented the validation of the model developed in DUST with respect to the existing helicopter simulator. Firstly, a brief insight on reference frames is presented, followed by the description of the model and the considered flight condition. Secondly, is described how to obtain comparable input and output between the two models. Lastly, results are presented.

2.1. Reference frames

A fundamental aspect of the validation process is the comprehension of the reference frames of the two models. While the DUST model only considers the rotor, the simulator model is of the complete helicopter; in the following, only the frames of interest will be presented.

2.1.1. Simulator

The results from the simulator [7] are presented with respect to the Hub fixed reference frame (HF), originated in the centre of the hub and tilted by a fixed angle I_θ along the pitch axis, with respect to the helicopter body frame (BY). While the offset between BY and HF will be of no relevance for the case, I_θ will be considered. The Hub rotating frame (HR) has the same origin and inclination of HF, y_{HR} is aligned to the eccentricity arm of the bth blade and rotates with respect to HF of $\left(-\psi_b + \frac{\pi}{2}\right)$ around z_{HF}, where ψ_b is the azimuthal position of blade b. The last reference frame of interest is the blade frame (B), which is also rotating. The origin of B is shifted by the eccentricity and, with respect to HR, is rotated following the rotation sequence $(-\beta \;\; 0 \;\; -\zeta)$, where β and ζ are respectively the flapping and the leading angle of blade b. HF, HR, and B are shown in Figure 2-1. Figure 2-2 Figure 1-1shows HF with respect to the whole helicopter, index BY identifies Body reference frame. The angle I_θ has been exaggerated for clarity.

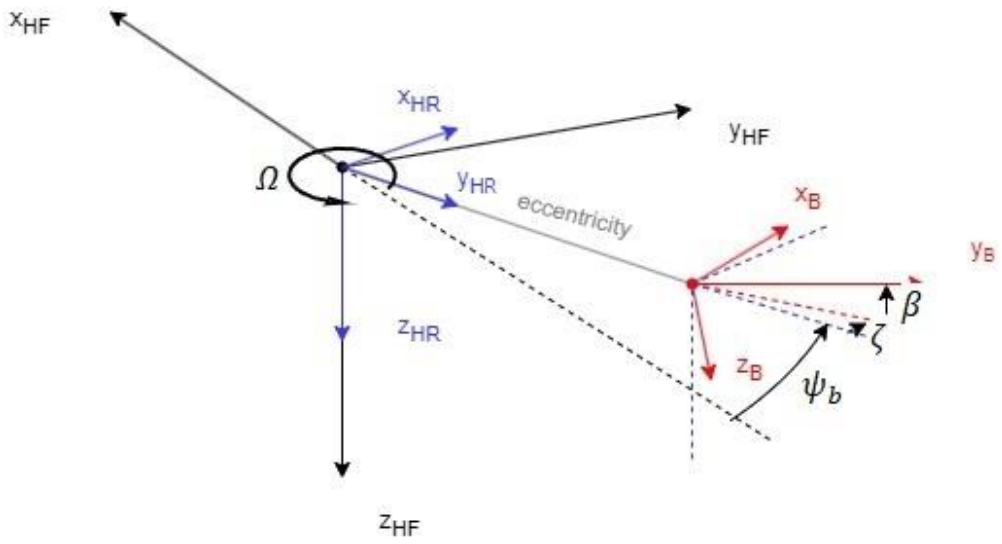

Figure 2-1 Reference frames, Simulator

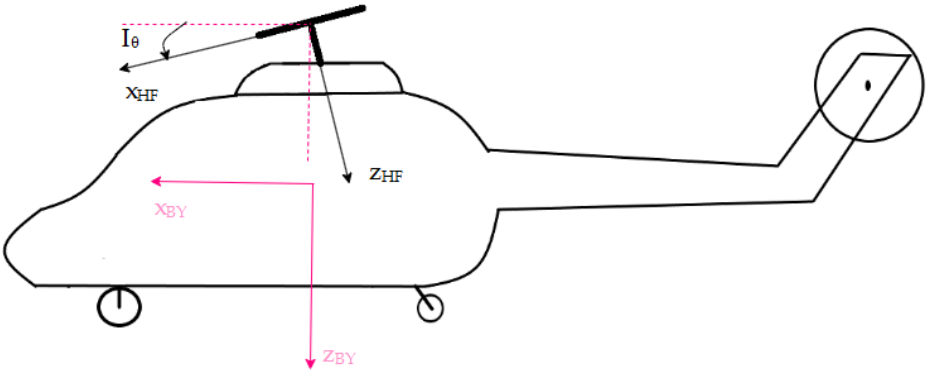

Figure 2-2 Full helicopter sketch, Simulator

2.1.2. DUST

The reference frames in DUST are defined in a hierarchical manner, starting from the internal, unmodifiable parent frame 0 [12], giving an origin offset and a rotation around an axis. The first frame manually defined is the one concerning the tilting of the hub. As previously stated, the body is not represented in this model, therefore the origin of the frame has been defined coincident with that of 0, while a rotation around y0 of angle Iθ has been performed. This frame D has been defined only for practicality, to easily modify the parameter Iθ; if needed, the tilting could have been defined directly in the Hub fixed frame. The Hub fixed frame (HF) has been defined over D, with no variation in origin nor orientation, exploiting the multiplicity option in DUST. This option allows to directly define a rotor giving the number of blades, the angular velocity, the offset between the centre of the hub and the root of the blades and the degrees of freedom of the blades. These parameters will be analysed in the following

paragraphs. DUST automatically defines the Hub rotating frame (HR) and a reference frame for each declared degree of freedom, performing a rotation and a translation based on the input parameters. The last of these frames corresponds to the blade frame (B). DUST reference frames are rotated of 180° around roll axis with respect to those described for the simulator. This discrepancy will be considered in the postprocessing of the results, to avoid the definition of a further reference frame. Free stream velocity is a parameter to be defined by the user, as is shown in the following. HF, HR, and B are shown in Figure 2-3.

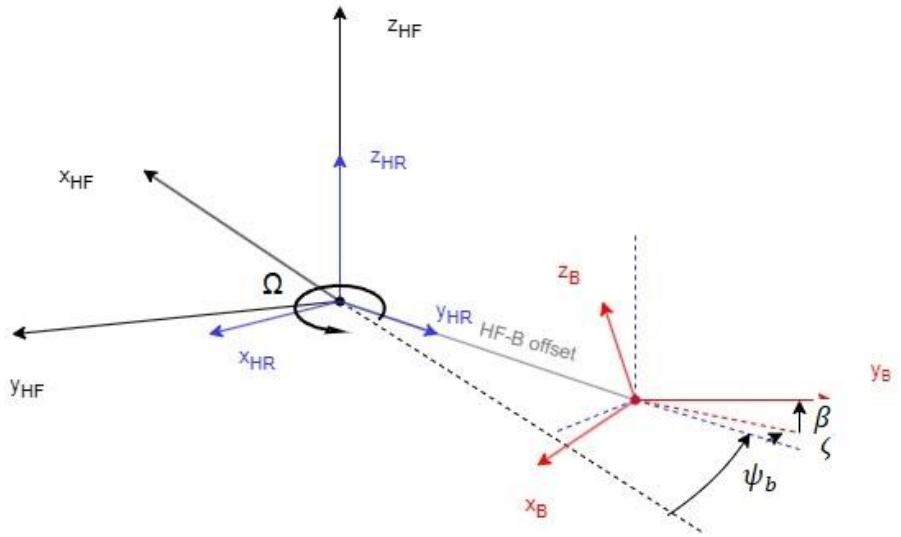

Figure 2-3 Reference Frames, DUST

2.2. Model definition

2.2.1. Rotor

As said in chapter 1.2, the model is based on a light utility helicopter. The rotor is articulated, with five blades. All the information needed for the model development is available from the simulator, as will be seen in the following paragraphs.

2.2.1.1. Blade

For this application it has been chosen to model the blade in DUST as a lifting line. The geometry of the blade in the simulator is described by 21 points. For each station the position r, scaled on the blade radius R ($r = 0$ is the root station and $r = 1$ the tip station), the chord and the twist of the section are defined. The blade is deigned over two different aerofoils, one from $r = 0$ to $r = 0.85$, and the other from $r = 0.851$ to $r = 1$. For both the aerodynamic coefficients C_L and C_D are available. The moment coefficient, which is also required by DUST, has been always imposed equal to 0.

The parametric geometry construction in DUST requires the definition of N section and N-1 regions. The input parameters are, respectively, chord, twist and aerofoil data, and length of the region, sweep and dihedral angles, and number of elements in the region and their distribution. The number of sections has been chosen based on the twist distribution along the blade length, shown in Figure 2-4, as the chord do not present abrupt changes.

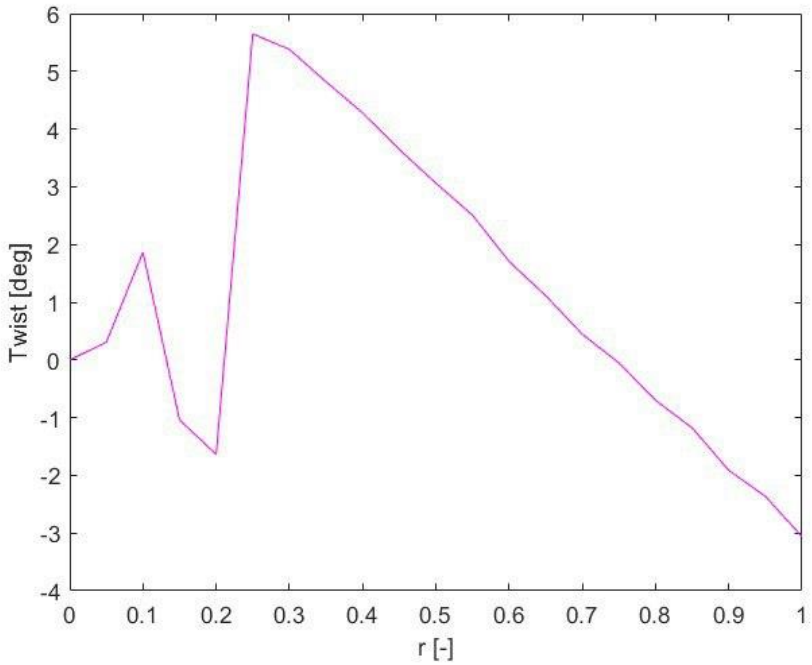

Figure 2-4 Blade twist

The blade has been divided in six sections:

- First section: root
- Second section r = 0.1
- Third section r = 0.2
- Fourth section r = 0.25
- Fifth section r = 0.85 (this section is not due to a change in twist, but due to the change of the aerofoil)
- Sixth section r = 1

In the five regions, the sweep and dihedral angle are left to 0, as they are of no use in this application, while the span of the n region is determined as in 2.1.

$$S_n = R * (r_{n+1} - r_n) \qquad 2.1$$

where r_n is the radial position of the n^{th} section. The elements of the span are uniformly distributed along the length of region, their number is obtained as in 2.2.

$$E_n = 5 * (r_{n+1} - r_n)/0.5 \qquad 2.2$$

After analysing the convergence of the results, the uniform distribution and the number of elements had been chosen, as the best combination of results quality and computational speed.

2.2.1.2. Hub

The inputs needed to define the geometry of the hub are the tilt angle I_θ, the radius and the eccentricity. All those parameters are available from the input of the simulator. DUST does not consider the hub as a physical entity, but only in terms of reference frame, therefore the values had to be introduced in terms of offsets and rotations. In the simulator all the hinges share the same position, at distance $\overline{HFh} = \frac{\emptyset}{2} + ecc$ from the centre of the Hub. The offset between HF and B has been taken directly equal to $\overline{HFh}$, meaning that the root of the blade and the three hinges share the same position. This choice has been made to have a coherent construction between the models and to include in DUST the blade root cut out present in the simulator. The rotational speed to be imposed to HR is Ω taken from the simulator outputs (a more detailed explanation will be presented in the following paragraphs).

2.2.2. Test conditions

The test condition has been obtained on the simulator, to which was required the trim point for the helicopter flying at constant speed and constant altitude. The inputs were weight (of no interest in DUST), altitude (1500 ft) and speed (65 kts). To achieve comparable results, all the contributions of the autopilot were switched off. The outputs needed for the DUST model were:

- The three components of the velocity of the helicopter u, v, w in m/s
- The flapping modes (β_0, β_{1c}, β_{1s}, β_{2c}, β_{2s}) in rad from multiblade coordinates
- The lag modes (ζ_0, ζ_{1c}, ζ_{1s}, ζ_{2c}, ζ_{2s}) in rad from multiblade coordinates
- Ω in rad/s
- The three pitch components θ_0, A_1, B_1 in rad/s
- The aerodynamic loads (forces and moments) at the hub. These loads are only due to aerodynamic effects. Mass, inertia, and dynamic contribution are not included.

2.3. Compatibility of the models

The two models are based on different approaches; therefore, some processing of input and output is needed.

2.3.1. Inputs

The velocity inputs u, v, w and Ω do not need any processing, as they are already compatible both in structure and in unit of measurement (respectively m/s and rad/s). The altitude can be imposed in terms of pressure, density, and speed of sound, according to the ISA.

A more careful processing is needed for flap, lag, and pitch. The simulator is based on a multiblade coordinate approach, where the generic degree of freedom of the blade can be expressed as 2.3

$$\nu_b = \nu_0 + \sum_n (\nu_{nc} \cos(n\psi_b) + \nu_{ns} \sin(n\psi_b)) \qquad 2.3$$

where ν is the degree of freedom of the b[th] blade, n goes from 1 to $n = (N-1)/2$, since the number of blades N is odd, and ψ_b is the azimuth angle of the blade. The reactionless modes (n>1) will be not considered in DUST as they do not cause any significant transfer of load to HF [13]. A more detailed explanation of multiblade coordinates can be found in Appendix A.

The degrees of freedom of the blade from the simulator for the case are flapping (2.4), lead-lag (2.5), and pitch (2.6).

$$\beta_b = \beta_0 + \beta_{1c} \cos(\psi_b) + \beta_{1s} \sin(\psi_b) \qquad 2.4$$

$$\zeta_b = \zeta_0 + \zeta_{1c} \cos(\psi_b) + \zeta_{1s} \sin(\psi_b) \qquad 2.5$$

$$\theta_b = \theta_0 + A_1 \cos(\psi_b) + B_1 \sin(\psi_b) \qquad 2.6$$

DUST requires the input in terms of a constant, an amplitude A_ν and a phase φ_ν, therefore the previous have been transformed in single cosine waveform as in 2.7 for flap, 2.8 for lag, and 2.9 for pitch.

$$\beta_b = \beta_0 + A_\beta \cos(\psi_b + \varphi_\beta) \quad 2.7$$

$$\zeta_b = \zeta_0 + A_\zeta \cos(\psi_b + \varphi_\zeta) \quad 2.8$$

$$\theta_b = \theta_0 + A_\theta \cos(\psi_b + \varphi_\theta) \quad 2.9$$

Phase and amplitude can be computed as in 2.10 and 2.11, respectively.

$$\varphi_\nu = -\tan^{-1}(\frac{\nu_s}{\nu_c}) \quad 2.10$$

$$A_\nu = \sqrt{{\nu_s}^2 + {\nu_s}^2} \quad 2.11$$

Moreover, the input was required in degrees, so a conversion was also needed. It is currently in development in DUST an option that will allow to impose the motion directly as a Fourier series, so in the future the multiblade input might be directly imposed.

2.3.2. Outputs

The aerodynamic loads at the hub are an available output of the simulator. As previously stated, the rotor is articulated, while forces are directly estimated from the blade loads, the moments are obtained as the sum of a moment M_a, obtained from aerodynamic forces and an elastic moment, that considers the contributions of flap and lag hinges as tortional springs. Inertial moment contribution is not included in the comparison. Firstly, because DUST does not consider mass and consequently inertial loads, secondly, because the considered inflow model only includes contribution from strictly aerodynamic loads. In the simulator the moments of interest are computed as in 2.12, 2.13, and 2.14.

$$M_a = \overrightarrow{ecc} \wedge \overrightarrow{F_{HR}} \quad 2.12$$

$$M_{hBx} = K_\beta * \beta - K_\beta * preconing \quad 2.13$$

$$M_{hBz} = K_\zeta * \zeta \quad 2.14$$

where M_{hB} is the hinge moment in the blade reference frame, K_β and K_ζ are the elastic coefficients, and preconing is an input parameter representing the preconing angle of the rotor. The comparable moments are obtained as 2.15.

$$M_{HF} = R_{R2F} * M_a + R_{R2F} * R_{B2R} * (-M_{hB}) \quad 2.15$$

where R_{R2F} is the rotation matrix from Hub rotating frame to Hub fixed frame and R_{B2R} is the rotation matrix from Blade frame to Hub rotating frame. Matrices are explicitly presented in Appendix A.

In DUST the hinges are not considered as physical entities, but only as the origin of the prescribed motion; therefore, the moment at the Hub in output is transmitted directly from the blade. Moreover, the elastic moment is not included. Consequently, the outputs must be processed in order to achieve comparable results.

The analysis in DUST has been performed over five complete rotations of the rotor, as has been observed that three rotations are needed for the convergence of the solution, with 40-time step per rotation.

For each reference frame of interest an output file with the loads computed at its origin is available. Moreover, at each time step, the position of the origin is identified through the nine components of the rotation matrix from 0 to the frame, and the three components of the offset vector from 0.

The loads are taken for each blade in B and HF. For each timestep the loads of n^{th} blade are computed as in 2.16, and 2.17.

$$F_{0n} = R'_{02Bn} * F_{bn} \quad 2.16$$

$$M_{an} = offset_{02Bn} \wedge F_{0n} \quad 2.17$$

M_{hB} is computed as in the simulator, with flap and lag angles for each blade obtained as in 2.18 and 2.19, respectively, and hinge moment at 0 as in 2.20.

$$\beta_n = \beta_0 + A_\beta \cos\left(\Omega * t + \varphi_\beta - \frac{2\pi}{N} * (n-1)\right) \quad 2.18$$

$$\zeta_n = \zeta_0 + A_\zeta \cos\left(\Omega * t + \varphi_\beta - \frac{2\pi}{N} * (n-1)\right) \quad 2.19$$

$$M_{h0n} = R'_{02Bn} * M_{hBn} \quad 2.20$$

Finally, the loads at the hub are obtained in 2.21, 2.22, 2.23, and 2.24.

$$F_{HF} = \sum_{n=1}^{N} R_{02HFn} * F_{0n} \quad 2.21$$

$$M_{HF} = \sum_{n=1}^{N} R_{02HFn} * (M_{an} + M_{h0n}) \quad 2.22$$

$$F = R_{D2S} * F_{HF} \quad 2.23$$

$$M = R_{D2S} * M_{HF} \quad 2.24$$

The final rotation has been performed to align HF in DUST to that of the simulator. The final loads are computed as the average loads over a complete rotation of the rotor.

2.3.3. Validation

As said the validation has been performed at trim conditions for forward flight as constant altitude at 65 knots. The final loads for the trim condition in the simulator and the DUST model are summarized in Table 2.1.

Table 2.1 Simulator and DUST loads

	Simulator	DUST
Fx [N]	557	897
Fy [N]	-597	-437
Fz [N]	-27620	-29264
Mx [Nm]	223	137
My [Nm]	-3351	-5562
Mz [Nm]	7472	5864

Results are generally aligned; discrepancies are due to the different models used in the two systems and the cumulative errors due to rotations. The wake of the rotor, represented by a first vortex panel (dark blue) and the following vortex particles (light blue), are shown in the figures. The validation of the model in the trim condition represents a solid base for the following, more complex analysis, that will concern manoeuvres. Wake is shown in Figure 2-5, Figure 2-6, and Figure 2-7.

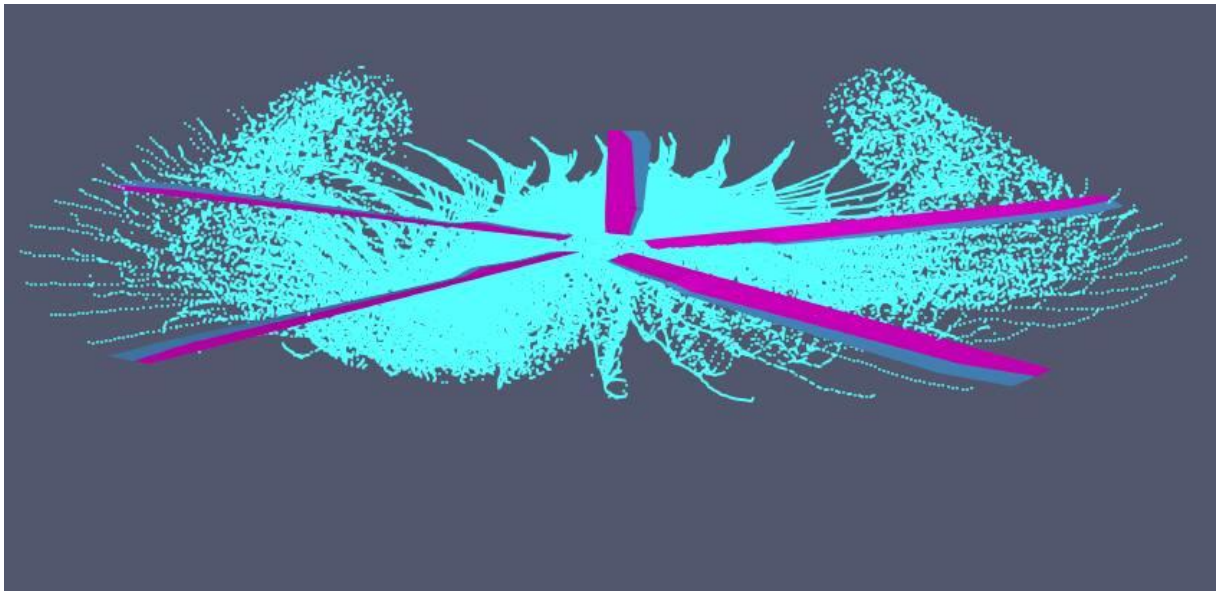

Figure 2-5 Wake (front view)

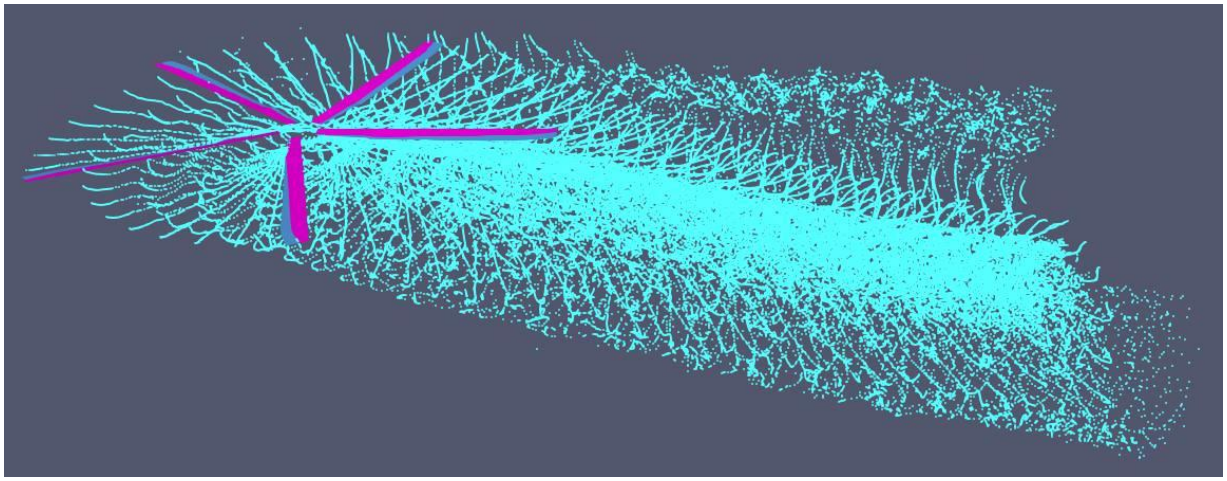

Figure 2-6 Wake (side view)

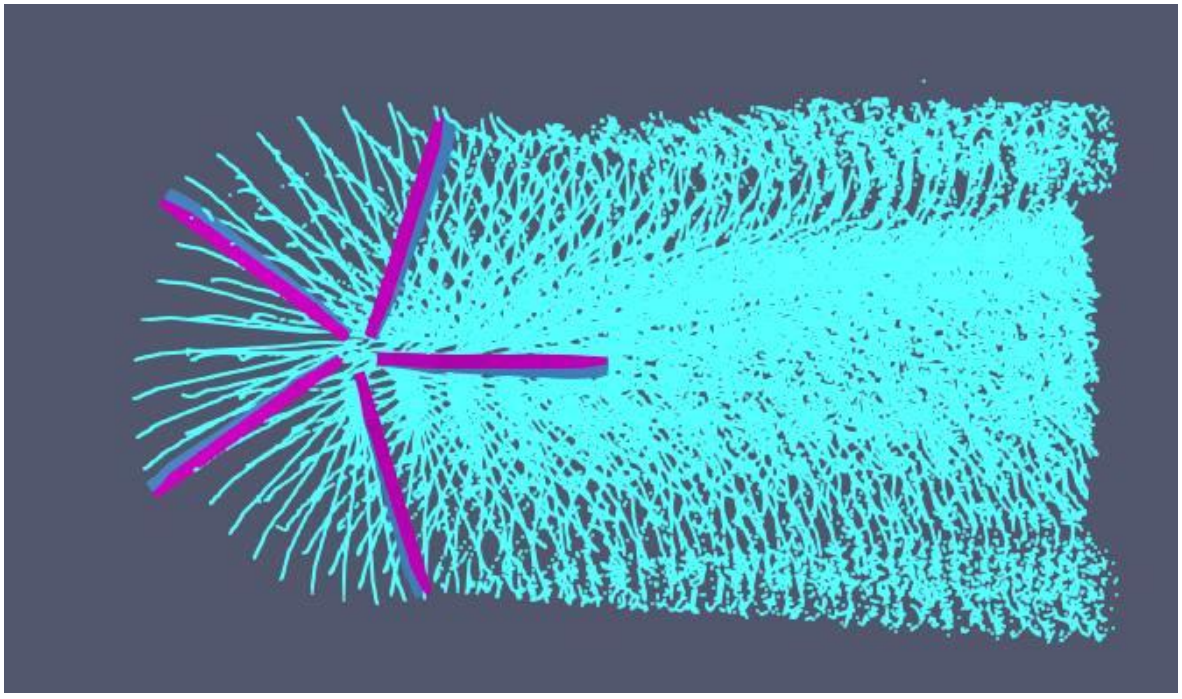

Figure 2-7 Wake (view from above)

3. New inflow model

In the following paragraphs the new inflow model is presented.

At first, the chosen manoeuvre is described, particularly how is obtained in the simulator, and implemented in DUST.

Secondly, DUST results are presented.

Thirdly, the new model is described and confronted with those obtained from the simulator and DUST.

Lastly, it is described how the new inflow model is implemented in the simulator.

3.1. Manoeuvre

The chosen manoeuvre is a mid-airspeed forward input. This manoeuvre covers a part of one of the validation tests for helicopter flight simulation training devices required by EASA [5], contained in section 2.c, concerning handling qualities. A summary of the table of FSTD validation tests can be found in Appendix C.

The manoeuvre starts at the trim conditions described in the previous chapter. After a second the cyclic longitudinal command is perturbed with a forward input, while all other commands are kept in the initial position (a small perturbation is seen on all commands due to coupled response). The new position of the longitudinal command is kept until the end of recording (Figure 3-1). As said the initial conditions are a forward speed of 65 knots at an altitude of 1500 ft.

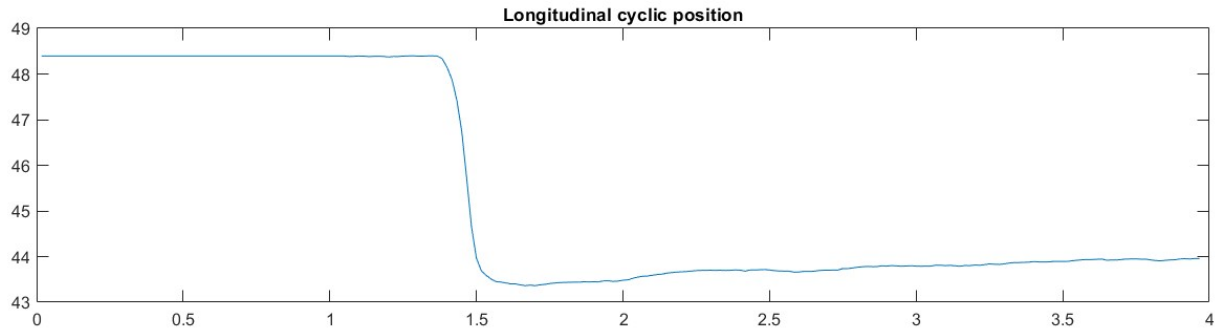

Figure 3-1 Longitudinal command input

While on the simulator the manoeuvre is dynamically represented, DUST only allows static input. It was therefore necessary to reconstruct the manoeuvre as a succession of trim points.

The initial timesteps from the simulator have been cut, as they do not include significant changes from trim condition, that has been taken as the initial point in DUST. Data from the final timestep have been taken as input for the concluding condition in DUST. Between these points, the manoeuvre has been divided in twenty focal points that have been used to reconstruct it on DUST. Each of the twenty-two steps has been constructed as the trim case presented in chapter 2. Moreover, three dummy reference frames have been constructed to include the contribution of angular velocity components of helicopter about fuselage x, y, and z axis, respectively p, q, and r, to introduce a dynamic correction.

The input from the simulator for each step are:

- The three components of the velocity of the helicopter u, v, w in m/s
- The three components of the angular velocity of the helicopter p, q, r in rad/s
- The flapping modes (β_0, β_{1c}, β_{1s}, β_{2c}, β_{2s}) in rad from multiblade coordinates
- The lag modes (ζ_0, ζ_{1c}, ζ_{1s}, ζ_{2c}, ζ_{2s}) in rad from multiblade coordinates
- Ω in rad/s
- The three pitch components θ_0, A_1, B_1 in rad/s

Each step inherits the initial condition from the previous, to grant continuity of the manoeuvre, thanks to a built-in option in DUST that allows to start the simulation from an existing output file.

3.2. DUST results

As described in chapter 2 the blade has been defined as a lifting line, with 105 sections along each blade. The radial position r and the circulation over the blade element γ of each section are available as outputs. Following lifting line theory, it is possible to compute the downwash contribution of each blade element as in 3.1.

$$w_b = \frac{\gamma}{4\pi r} \tag{3.1}$$

It is therefore possible to obtain the downwash along the blade at each timestep. The obtained downwash is shown in Figure 3-2, Figure 3-3, Figure 3-4, Figure 3-5, and Figure 3-6, where blades are positioned as represented in Figure 3-7.

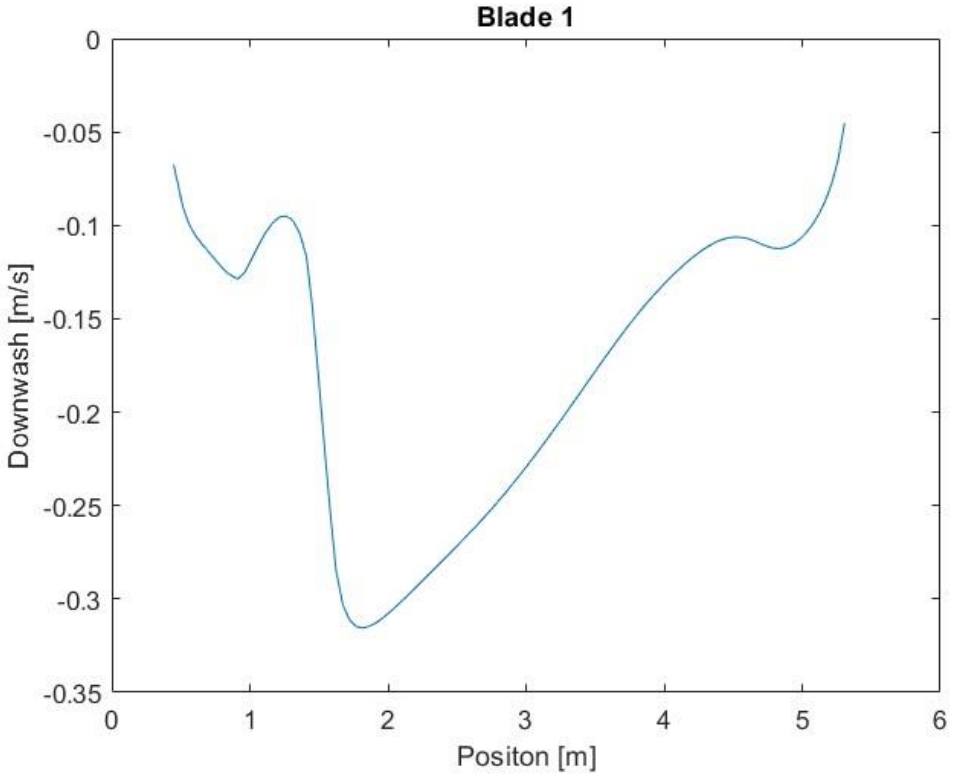

Figure 3-2 Downwash on blade 1

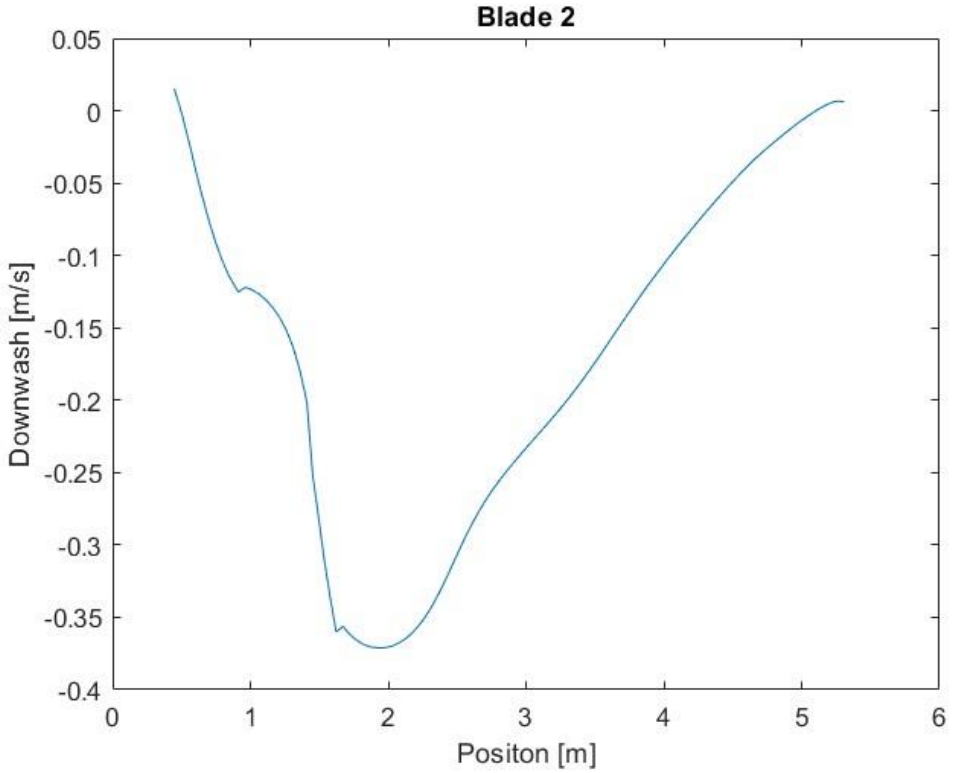

Figure 3-3 Downwash on blade 2

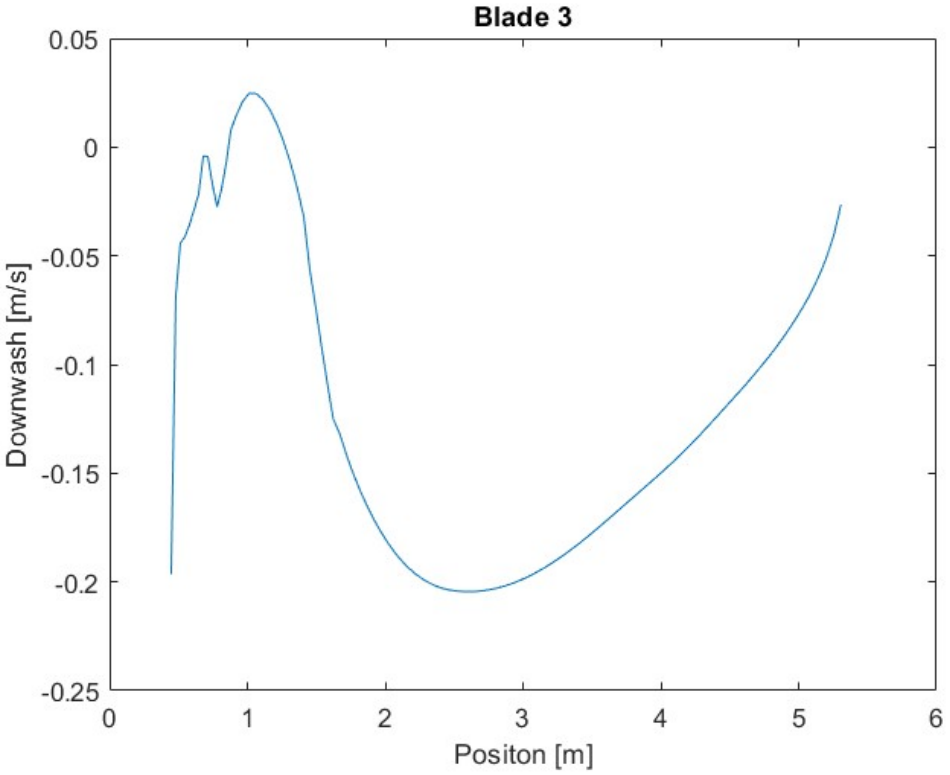

Figure 3-4 Downwash on blade 3

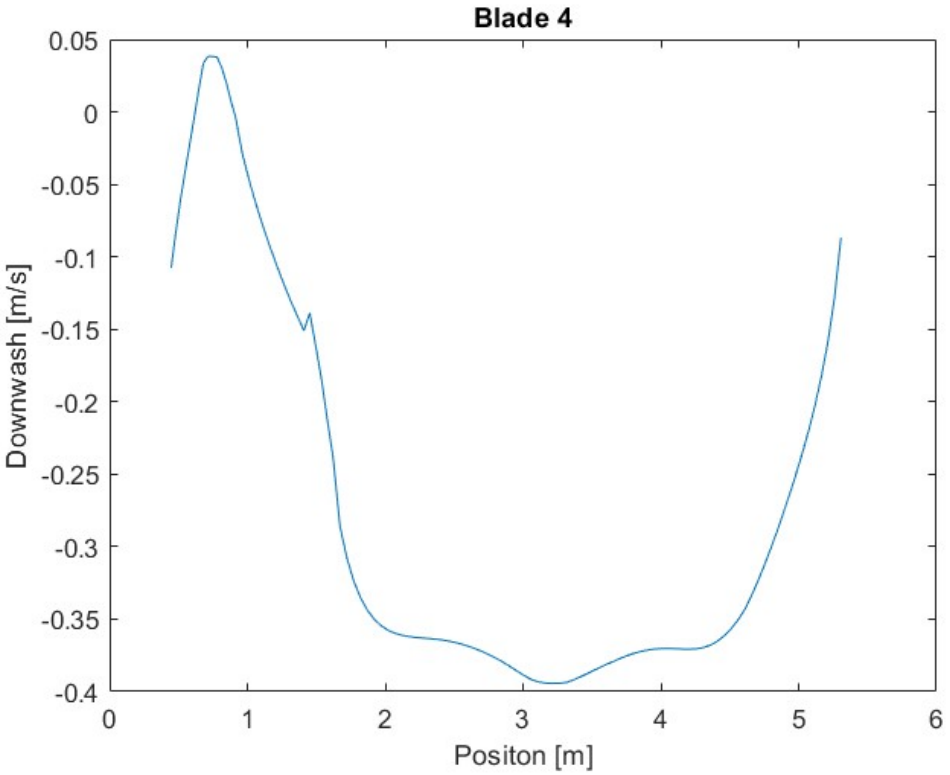

Figure 3-5 Downwash on blade 4

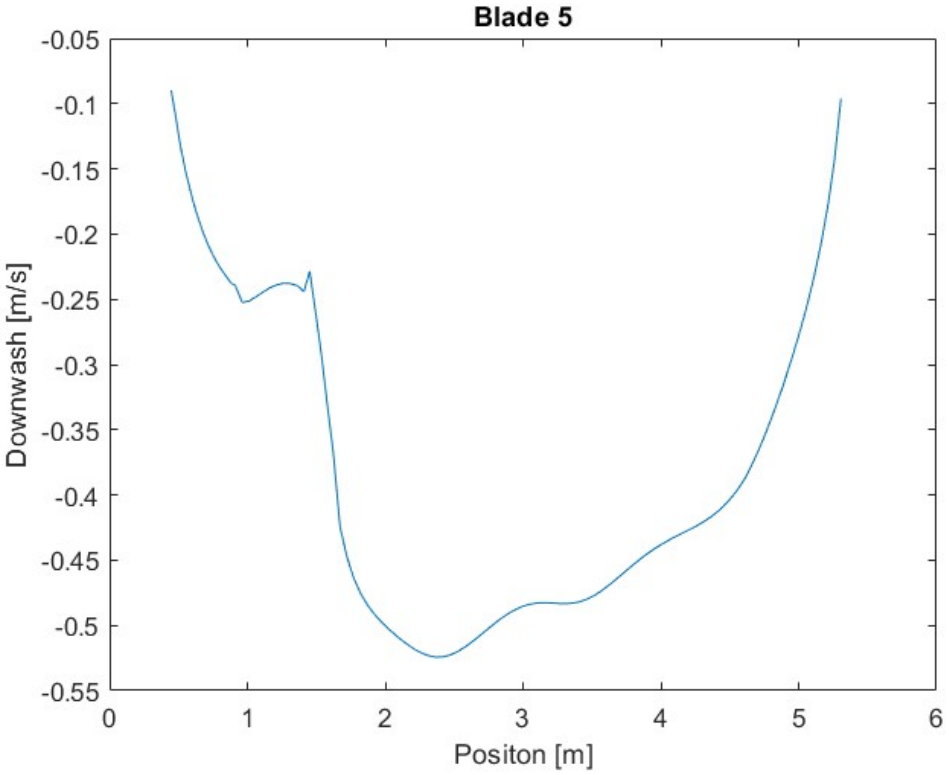

Figure 3-6 Downwash on blade 5

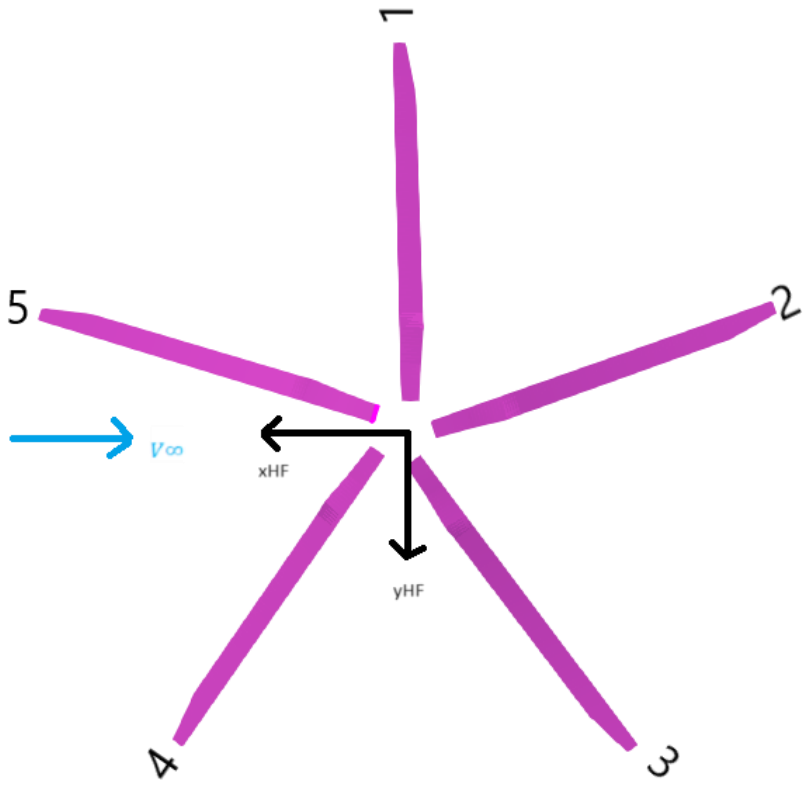

Figure 3-7 Position of blades

As can be seen results are highly non-linear and cannot be directly used in the simulator. Moreover, this model correctly represents aerodynamic effects over retreating blades, particularly visible on blades 3 and 4 in Figure 3-4, Figure 3-5. The polar representation of the inflow of the whole rotor is shown in Figure 3-8. To introduce DUST model into the simulator, it is necessary to linearize it.

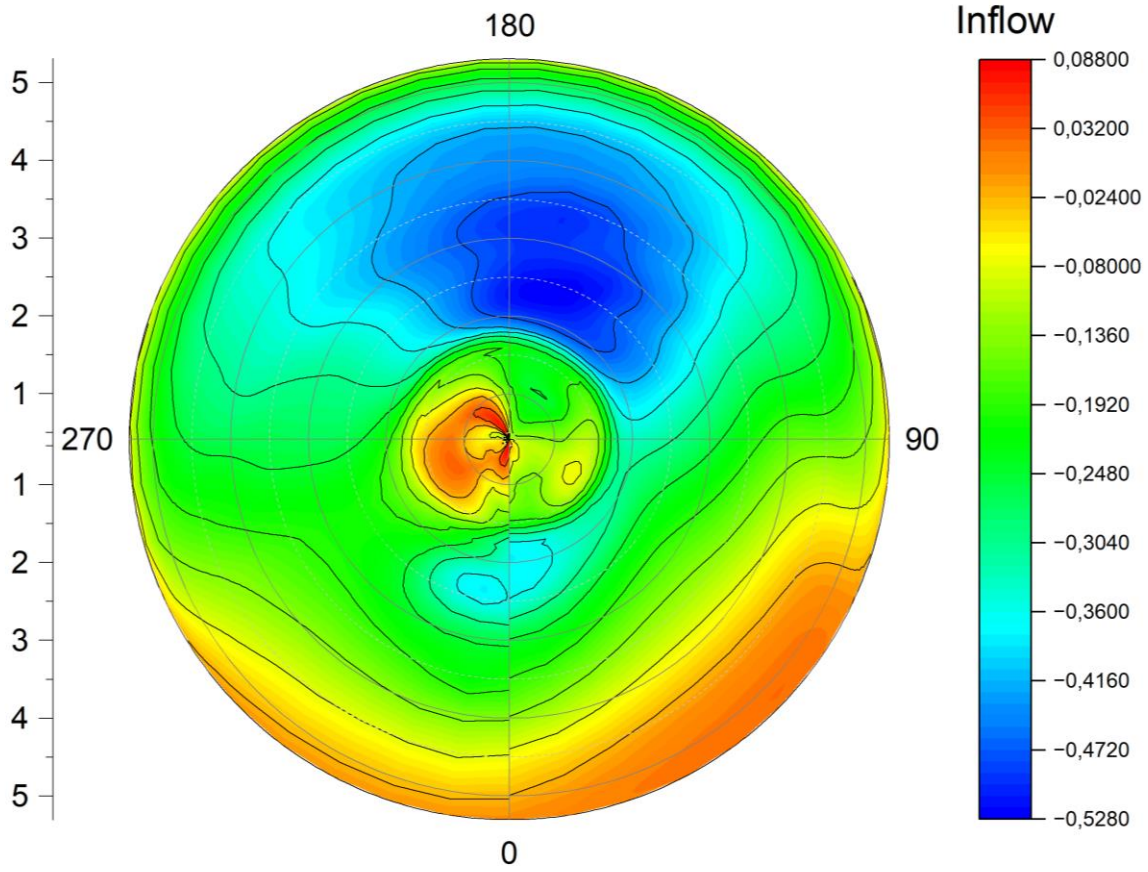

Figure 3-8 Inflow

3.3. Linearized inflow model

As said, the linearized inflow model is a simplified model that represents the inflow as a sum of a component λ_0, that represents the average inflow over the rotor disk, and two contributions, that represent the longitudinal and lateral variation, depending on the inflow distribution and the blade element position, as in 3.2

$$\lambda = \lambda_0 + r(\lambda_s \sin\psi + \lambda_c \cos\psi) \qquad 3.2$$

Where r is the radial position of the blade element scaled on blade radius, going from 0 (blade root), to 1 (blade tip), ψ is the azimuth angle and λ_c and λ_s are, respectively, the longitudinal and the lateral variation of the inflow. To obtain the three states model needed in the simulator it is necessary to extract λ_0, λ_c and λ_s from the DUST inflow model as in 3.3, 3.4, and 3.5.

$$\lambda_0^n = \frac{1}{2\pi}\int_0^{2\pi}\int_0^1 r w_n \, dr d\psi \qquad 3.3$$

$$\lambda_c^n = \frac{1}{\pi}\int_0^{2\pi}\int_0^1 r w_n \cos(n\psi)\, dr d\psi \qquad 3.4$$

$$\lambda_s^n = \frac{1}{\pi}\int_0^{2\pi}\int_0^1 r w_n \sin(n\psi)\, dr d\psi \qquad 3.5$$

Where w_n is the inflow generated by the elements n^{th}blade, varying with radial position and azimuth angle, over an entire rotation. Finally, the three inflow states have been computed as the average for the five blades [3]. For blades positioned as in Figure 3-7, the three different inflow model are shown in Figure 3-9, Figure 3-10, Figure 3-11, Figure 3-12, and Figure 3-13. The blue line represents the complex DUST model, the red line is the reconstructed inflow model, and the yellow line is the simulator model.

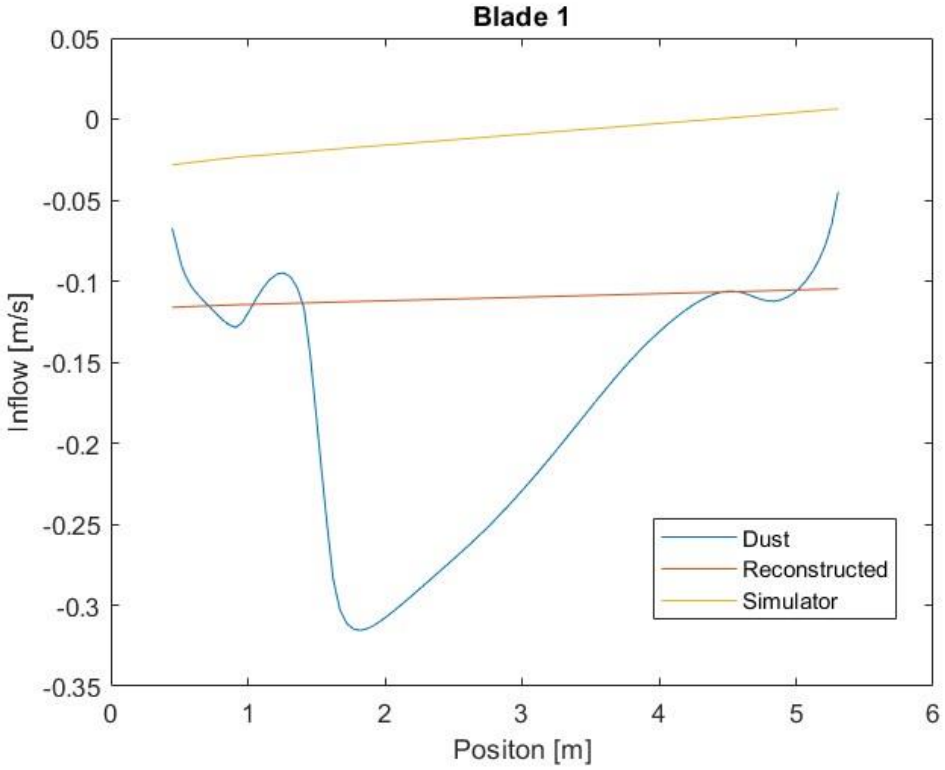

Figure 3-9 Confront of the three model on blade 1

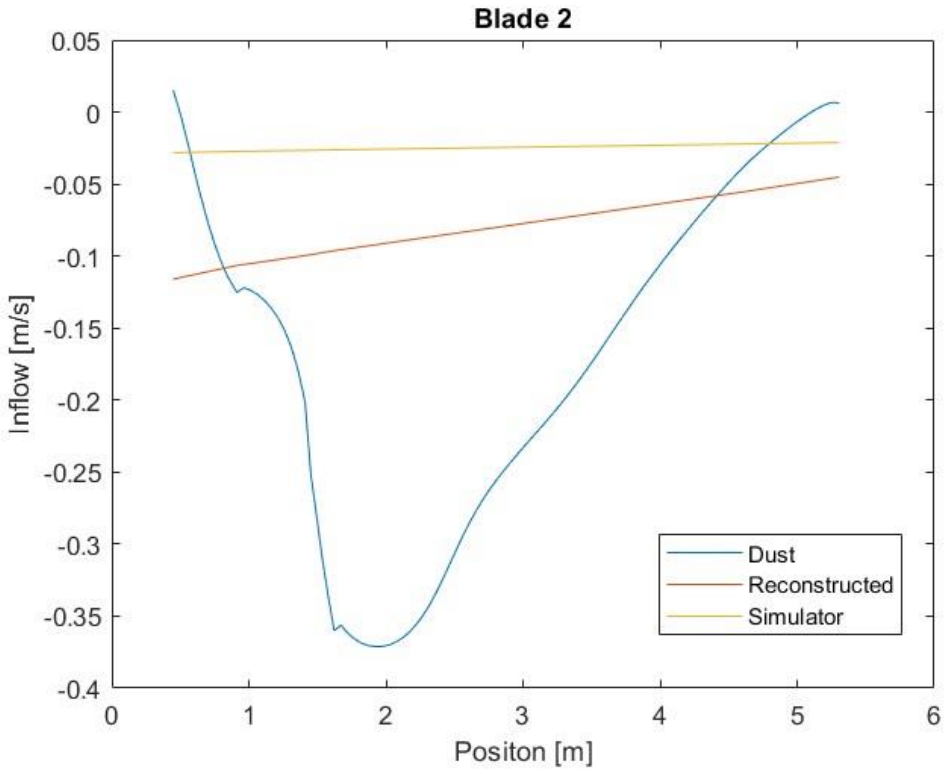

Figure 3-10 Confront of the three model on blade 2

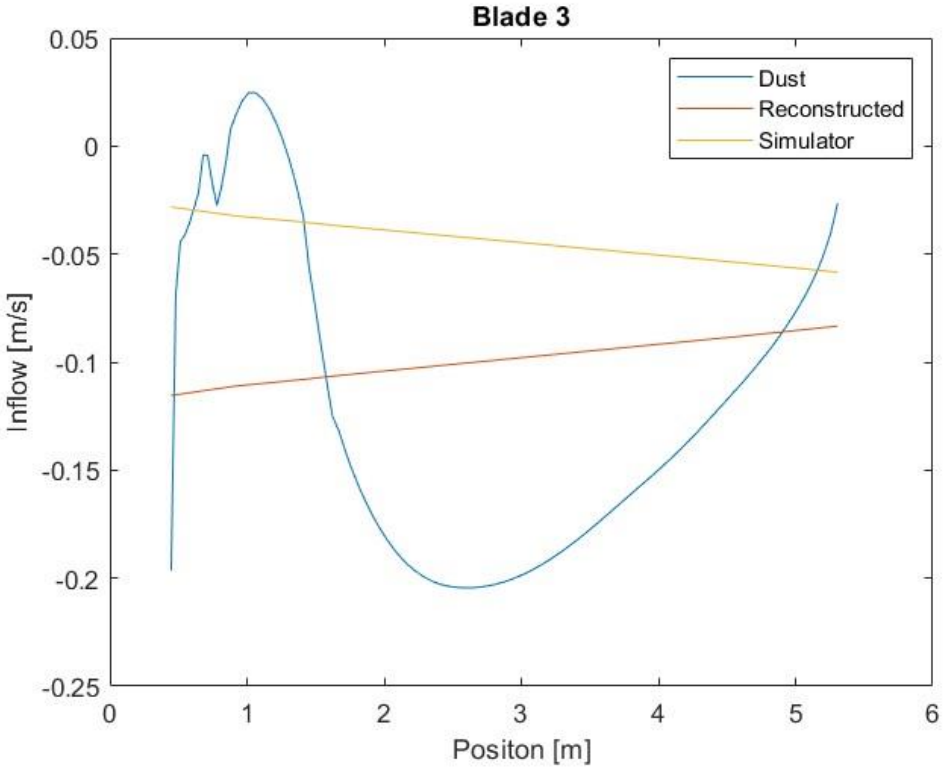

Figure 3-11 Confront of the three model on blade 3

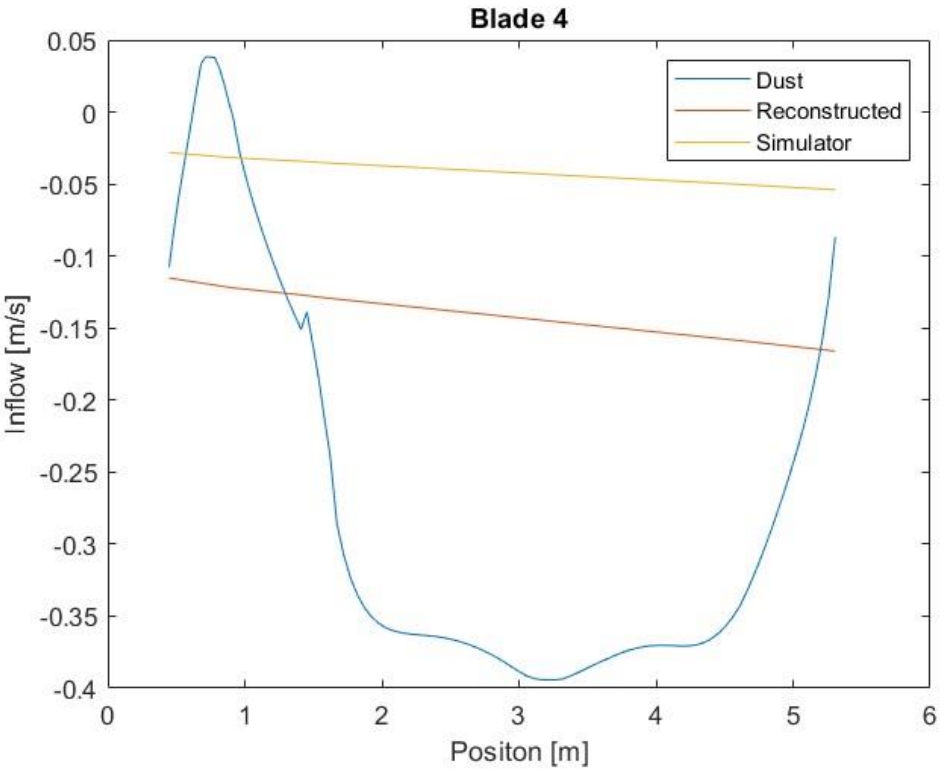

Figure 3-12 Confront of the three model on blade 4

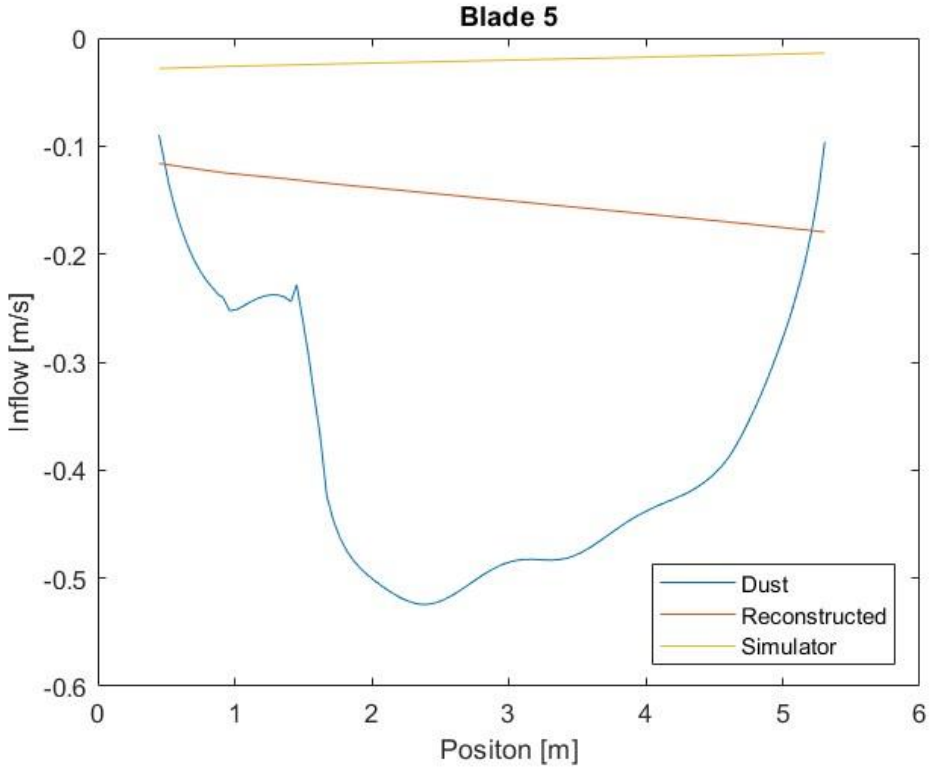

Figure 3-13 Confront of the three model on blade 5

It is immediately visible how the two linear models are unable to represent complex aerodynamic effects, such as root and tip effects and inverse flow on retroceding blades. Nevertheless, the reconstructed model is indirectly impacted by those phenomena and as expected, behaves differently from the simulator model. This is particularly visible over blade 3 (Figure 3-11), where the flow inversion leads to opposite behaviors.

3.4. System identification

Once obtained the linear model, for each step of the maneuver the aerodynamic loads and the three inflow states are available. The model implemented in the simulator requires the coefficients, obtained from the thrust, the roll moment, and the pitch moment as in 3.6, 3.7, and 3.8, respectively.

$$C_T = {F_z}/{\rho\pi\Omega R^4} \tag{3.6}$$

$$C_l = {M_x}/{\rho\pi\Omega R^5} \tag{3.7}$$

$$C_m = {M_y}\Big/{\rho\pi\Omega R^5} \tag{3.8}$$

Where ρ is the air density at the chosen altitude according to ISA, Ω is the rotational speed and R is the blade radius. To introduce the new model in the simulator the components of the L matrix are needed. Since inputs, outputs and structure of the model are known, the best approach is to use grey-box model identification [14]. A general linear, time invariant, state-space grey-box model is described in 3.9.

$$\begin{aligned} \dot{\boldsymbol{x}}(t) &= A\boldsymbol{x}(t) + B\boldsymbol{u}(t) \\ \boldsymbol{y}(t) &= C\boldsymbol{x}(t) + D\boldsymbol{u}(t) + \boldsymbol{v}(t) \end{aligned} \tag{3.9}$$

Where **x** is the vector containing the states of the system, **u** is the input vector, **y** the output vector, and **v** the disturbance vector.

The time discrete representation of the same model, particularly useful in case of limited time steps, is shown in 3.10.

$$\begin{aligned} \boldsymbol{x}(k+1) &= A\boldsymbol{x}(k) + B\boldsymbol{u}(k) \\ \boldsymbol{y}(k) &= C\boldsymbol{x}(k) + D\boldsymbol{u}(k) + \boldsymbol{v}(k) \end{aligned} \tag{3.10}$$

For the present inflow model the system becomes 3.11

$$\begin{Bmatrix} \lambda_0(k+1) \\ \lambda_s(k+1) \\ \lambda_c(k+1) \end{Bmatrix} = \begin{bmatrix} L_{11} & 0 & L_{13} \\ 0 & L_{22} & 0 \\ L_{31} & 0 & L_{33} \end{bmatrix} \begin{Bmatrix} \lambda_0(k) \\ \lambda_s(k) \\ \lambda_c(k) \end{Bmatrix} + \begin{bmatrix} 1 & 0 & 0 \\ 0 & 1 & 0 \\ 0 & 0 & 1 \end{bmatrix} \begin{Bmatrix} C_T(k) \\ C_l(k) \\ C_m(k) \end{Bmatrix} \tag{3.11}$$

$$\begin{Bmatrix} y_0(k) \\ y_1(k) \\ y_2(k) \end{Bmatrix} = \begin{bmatrix} 1 & 0 & 0 \\ 0 & 1 & 0 \\ 0 & 0 & 1 \end{bmatrix} \begin{Bmatrix} \lambda_0(k) \\ \lambda_s(k) \\ \lambda_c(k) \end{Bmatrix}$$

Noise has not been taken into account and the matrix C has been written as the identity matrix so that the output vector coincides with the state vector. The nonzero values of matrix A, i.e., L_{11}, L_{13}, L_{22}, L_{31}, and L_{33} are the five parameters that need to be identified.

The initial condition, **x**(k = 0), has been taken equal to the states vector for the first step, while data from the following 21 steps has been used for the system identification.

To estimate the five parameter MATLAB® functions ***idgrey*** and ***greyest*** have been exploited [15] [16]. The first function allows the user to define either a continuous or, as in this case, a discrete model. The second function allows the user to define which parameters from the defined model are fixed and which are those to estimate, based on the given dataset. ***greyest*** also allows the user to define other options for the estimation process such as the initial state, the maximum number of iterations to convergence and the estimation method.

The best result (Figure 3-14) has been obtained in 21 iterations (with the limit raised from the default 20 to 50) and with the Levenberg-Marquardt method [17] (a brief explanation of this method can be found in appendix C).

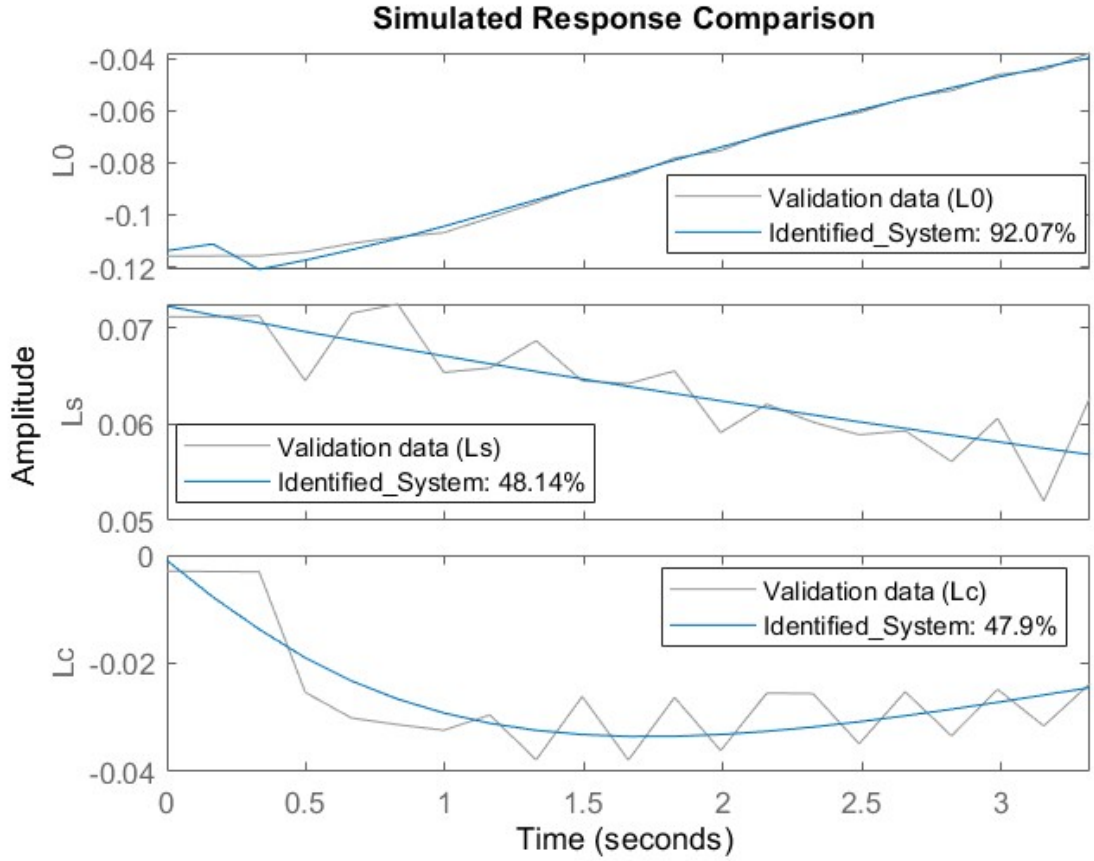

Figure 3-14 Compare between Data and identified system

The obtained parameters have been introduced in the simulator in place of the old matrix L that included the wake correction. Therefore, the new inflow model would not present any correction to obtain a better insight of the potential of the vortex particle method.

Results are presented in the following chapter.

4. Conclusion and future developments

In this chapter the conclusion of this thesis work is presented.

Firstly, results are discussed, lastly lesson learned, and possible future developments are presented.

4.1. Results

The estimated parameters have been introduced in the simulator in the matrix L. As described in 1.2.1, the existing inflow model included dependence on wake angle χ, and a wake corrective contribution δL added to L, while the new model only includes fixed parameters and has the form in 1.3, where [M] keeps the form in 1.4 and [L] becomes 4.1.

$$\begin{bmatrix} L_{11} & 0 & L_{13} \\ 0 & L_{22} & 0 \\ L_{31} & 0 & L_{33} \end{bmatrix} \qquad 4.1$$

To compare the results with the two inflow models, the manoeuvre in 3.1 has been repeated twice: a first time with the new inflow model and the second time with the original inflow, but without the wake correction. Results for pitch and roll (both in angle and rate) are shown in Figure 4-1, Figure 4-2, Figure 4-3, and Figure 4-4, respectively. The blue line represents data from the real helicopter, the red line shows the results obtained with the original simulator inflow model with wake correction, the yellow line follows the new inflow results, and finally, the purple line represents the original model without wake correction.

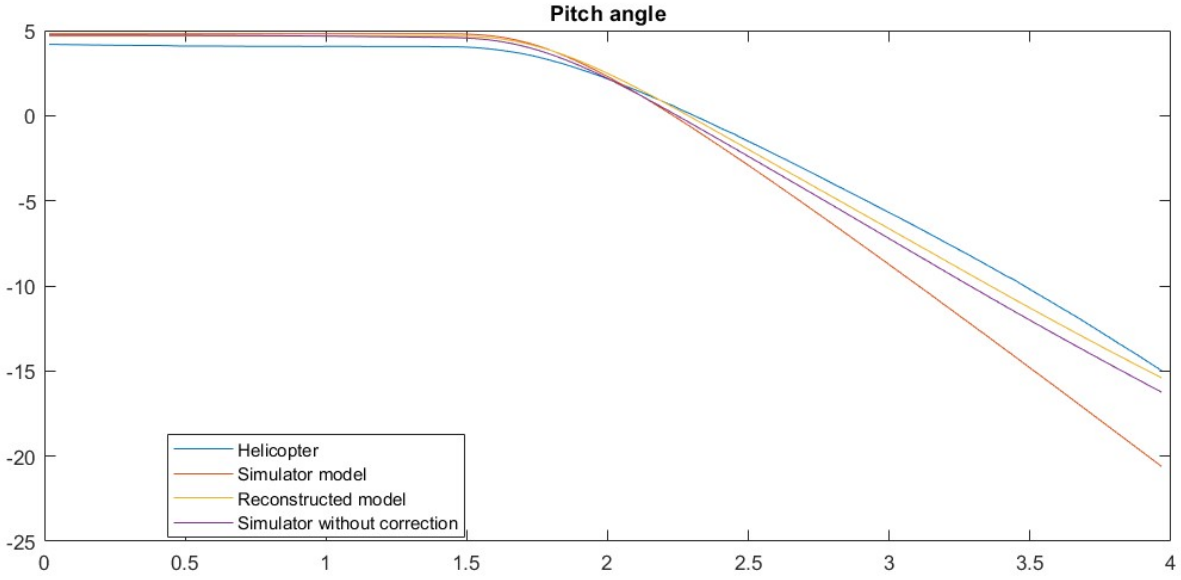

Figure 4-1 Pitch angle

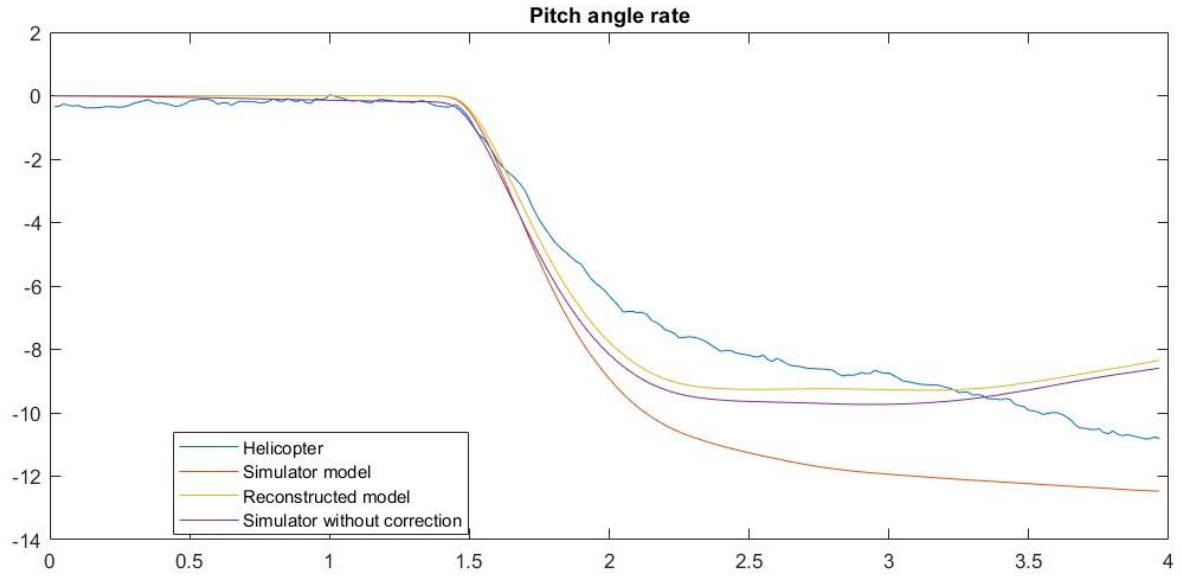

Figure 4-2 Pitch rate

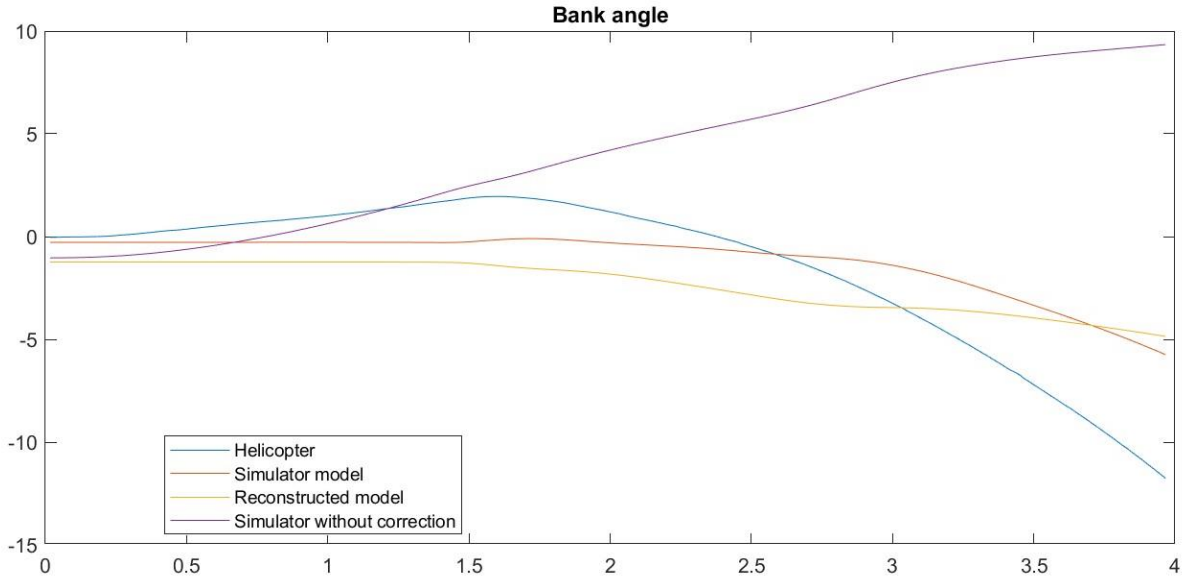

Figure 4-3 Bank angle

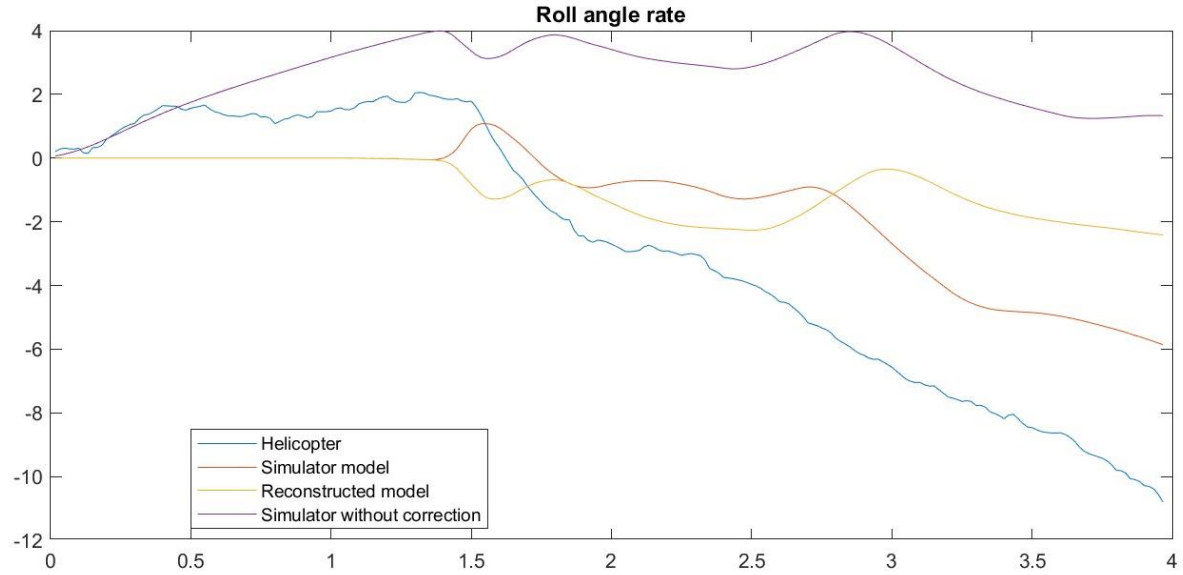

Figure 4-4 Roll rate

It is noticeable that, while all the simulated results are close for pitch angle, the bank angle for the simulator without wake correction is in clear opposition with the helicopter baseline. Such a result is expected and well demonstrates the known limitations of the Pitt-Peters model concerning the off-axis response.

The new inflow model improves the fidelity over pitch angle and is aligned with the original model for the bank angle. This result shows the great potential of the vortex particle method, as it has been able to correctly follow the traced manoeuvre without any external intervention.

Moreover, the DUST model has been obtained following the dynamic imposed by the original model, which was already far from the helicopter results; therefore, the error with respect to the baseline was expected.

4.2. Future developments

While the obtained results show the feasibility of pairing a helicopter simulator with a medium fidelity solver based on vortex particle method, they also underline the importance of improvement.

Firstly, an immediate solution would be to use higher number of states to represent the inflow variations. As visible in Figure 3-9, Figure 3-10, Figure 3-11, Figure 3-12, and Figure 3-13, the use of three states leads to linear distribution of the inflow along the blade, therefore cutting many aerodynamic effects. This solution might be impractical, though, due to the strict time requirements of real time simulation and high computational that a five or more states system would have.

Another possible improvement would be to couple DUST with a dynamical solver. As seen in Figure 4-3 the solution is highly influenced by the error already present in the simulator. The use of inputs derived from a more complex dynamic, i.e., from a multibody solver, could lead to better results, unbiased by the inevitable error of a low fidelity solver. Multiple examples of such a procedure are already present in literature (i.e., [18]). While this solution could lead to accurate results, the coupling of the solver could lead to time consuming simulations, requiring an excessive amount of time to cover all the significant manoeuvres that can be performed in a simulator.

A last improvement could be to introduce in DUST the complete model of the helicopter. This solution would allow to fully exploit the potential of the VPM, including wake effects and interference due to aerodynamic surfaces, body, and tail rotor directly in the solver. While this solution would improve not only the inflow model, but also the wake correction, it would need a deep knowledge of the helicopter geometry. This would fail the requirement of generality of GFM simulators and would also need complex and time consuming CFD analysis.

4.3. Conclusion

Vortex particle method has proven to be a powerful tool to improve the quality of inflow and wake modelling in simulation. The flexibility of this method opens many ways to exploit it, all sharing a common obstacle: computational time. The trade-off between accuracy and needed time still pends toward more traditional method, with limitations that are already well known and, therefore, correctable, or circumventable. The continuous growth of technology, though, has already started to overcome these limitations, and mid fidelity solver as DUST will soon play fundamental role, with the goal of a direct, real time coupling with simulators.

Bibliography

[1] NATO, "Rotorcraft Flight Simulation Model Fidelity Improvement and Assessment," 2021.

[2] M. Gladfelter, C. He, C. Chang, M. B. Tischler, M. J.S.Lopez and O. Juhasz, "Enhancement and Validation of VPM-Derived State-Space Inflow Models for Multi-Rotor Simulation," 2020.

[3] C. He, M. Syal, M. B. Tischler and O. Juhasz, "State-Space Inflow Model Identification from Viscous Vortex Particle Method for Advanced Rotorcraft Configurations," 2017.

[4] J. D. Keller, J. Robert M. McKillip, D. A. Wachspress, M. B. Tischler and O. Juhasz, "A Free Wake Linear Inflow Model Estraction Procedure for Rotorcraft Analysis," 2017.

[5] European Aviation Safety Agency, Certification Specifications for Helicopter Flight Simulation CS-FSTD(H), 2012.

[6] R. Hull, "Development of a Rotorcraft/Propulsion Dynamics, Interface Analysis: Volume I," 1982.

[7] L. Pietrolati, *Improvement of Main Rotor Model for Commercial Full Flight Helicopter Simulator*, Torino: Politecnico di Torino, 2022.

[8] D. A. Peters and N. HaQuang, "Technical Note: Dynamic Inflow for Practical Applications," 1988.

[9] D. M. Pitt and D. A. Peters, "Rotor Dynamic Inflow Derivates and Time Constant from Various Inflow Models," 1983.

[10] G. D. Padfield, Helicopter Flight Dynamics, Including a Treatment of Tiltrotor Aircraft, Third Edition ed., 2018.

[11] M. Tugnoli, D. Montagnani, M. Syal, G. Droandi and A. Zanotti, "Mid-fidelity approach to aerodynamic simulations of unconventional," 2021.

[12] D. Montagnani, M. Tugnoli, F. Fonte, A. Savino, A. Cocco and A. Colli, *DUST User Manual,* 2022.

[13] W. Johnson, Helicopter Theory, New York: Dover Publications,Inc., 1980.

[14] J. Řehoř and V. Havlena, "A Practical Approach to Grey-box Model Identification," in *18th World Congress of The International Federation of Automatic Control*, Milano, 2011.

[15] "MathWorks Help Center: idgrey," [Online]. Available: https://it.mathworks.com/help/ident/ref/idgrey.html.

[16] "MathWorks Help Center: greyest," [Online]. Available: https://it.mathworks.com/help/ident/ref/greyest.html.

[17] V. Klein and E. A. Morelli, Aircraft System Identification. Theory and Practice, Reston: American Institute of Aeronautics and Astronautics, Inc., 2006.

[18] A. Cocco, A. Savino, A. Zanotti, A. Zanoni, P. Masarati and V. Muscarello, "Coupled Multibody-Mid Fidelity Aerodynamic Solver for Tiltrotor Aeroelastic Simulation," 2021.

A Appendix A

In the following, a brief description of multiblade coordinates will be provided.

A.1. Multiblade coordinates transformation

The motion of the blades can be represented through a set of coordinates that follows the blade, the Individual Blade Coordinates (IBCs). The combined effect of the blades on the rotor disc can be expressed in a fixed frame through disc coordinates or MultiBlade Coordinates (MBCs) [10],. Without any approximation it is possible to reconstruct MBCs from IBCs as in the following equations. The inverse process is also possible.

$$\nu_0 = \frac{1}{N_b}\sum_{i=1}^{N_b}\nu_i \tag{A.1}$$

$$\nu_{0d} = \frac{1}{N_b}\sum_{i=1}^{N_b}\nu_i(-1)^i \tag{A.2}$$

$$\nu_{jc} = \frac{1}{N_b}\sum_{i=1}^{N_b}\nu_i \cos j\psi_i \tag{A.3}$$

$$\nu_{js} = \frac{1}{N_b}\sum_{i=1}^{N_b}\nu_i \sin j\psi_i \tag{A.4}$$

Where ν is a generic degree of freedom, N_b is the number of blades and ψ_i is the azimuthal position of the i^{th} blade, computed as A.5

$$\psi_i = \psi + i\Delta\psi \tag{A.5}$$

Where ψ is the dimensionless time variable (for a helicopter with constant rotational speed $\psi = \Omega t$) and $\Delta\psi$ is the azimuthal spacing between blades $\Delta\psi = 2\pi/N_b$; j depends on the number of blades and its value varies from 1 to n as in A.6.

$$\begin{cases} n = \dfrac{(N_b - 1)}{2} \; for\ odd\ N_b \\ n = \dfrac{(N_b - 2)}{2} \; for\ even\ N_b \end{cases} \tag{A.6}$$

A.2. Physical interpretation

MBCs represent the disk mode shapes, particularly, ν_0 (A.1) is the collective mode, ν_{1c} (A.3) and ν_{1s} (A.2) are the cyclic modes, the longitudinal and the lateral respectively. All other components (i.e., ν_{jc} and ν_{js} for $j > 1$ and ν_{0d} (A.4)) are called the reactionless modes. In axial flow only cyclic and collective modes couple with the fixed system, while reactionless modes only represent internal motion. In nonaxial flow contribution to the fixed system come from every mode, but the dominant contribution still derives from cyclic and collective ones [13]. Moreover, the reactionless mode ν_{0d} is only present in rotors with an even number of blades. A graphic representation of MBCs is shown in Figure A-1,where the considered degree of freedom is flapping. MBCs are function of time, just as IBCs, and represent exactly the same motion. It is therefore possible to change from one coordinate system to the other at any time.

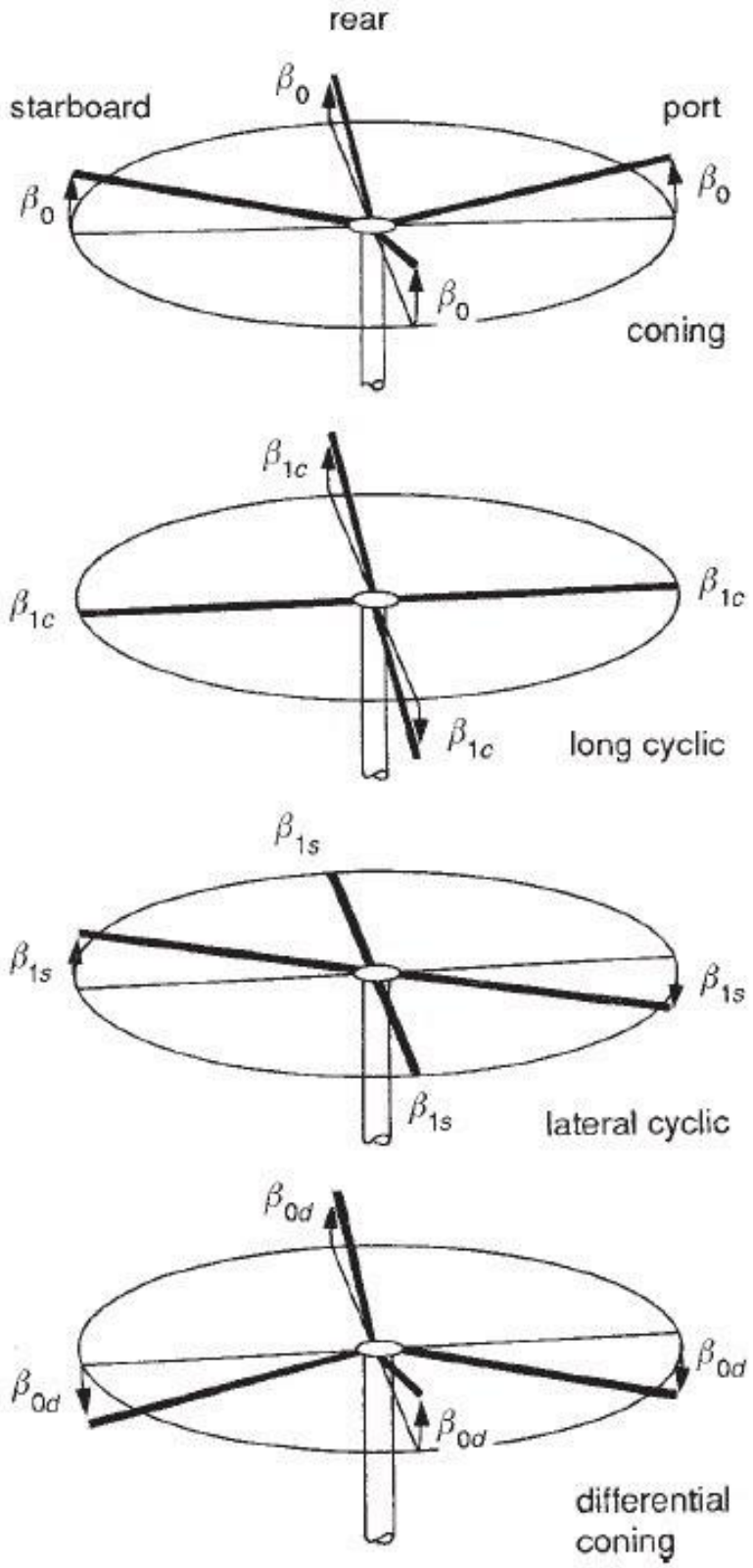

Figure A-1 Flapping motion in MBCs [10]

B Appendix B

In the following paragraphs will be presented the rotation matrices used.

B.1. Simulator

B.1 shows rotational matrix from Hub fixed to Hub rotating reference frame

$$R_{F2R} = \begin{bmatrix} cos(\psi_b - \frac{\pi}{2}) & sin(\psi_b - \frac{\pi}{2}) & 0 \\ -sin(\psi_b - \frac{\pi}{2}) & cos(\psi_b - \frac{\pi}{2}) & 0 \\ 0 & 0 & 1 \end{bmatrix} \quad \text{B.1}$$

B.2 shows rotational matrix from Hub rotating to Blade reference frame

$$R_{R2B} = \begin{bmatrix} cos(\zeta) & sin(\zeta) & 0 \\ -cos(\beta) * sin(\zeta) & cos(\beta) * cos(\zeta) & sin(\beta) \\ sin(\beta) * sin(\zeta) & -sin(\beta) * cos(\zeta) & cos(\beta) \end{bmatrix} \quad \text{B.2}$$

B.2. DUST

B.3 shows rotational matrix from 0 to Hub reference frame

$$R_{02H} = \begin{bmatrix} cos(\ I_\theta\ ) & 0 & sin(I_\theta) \\ 0 & 1 & 0 \\ -sin(I_\theta) & 0 & cos(I_\theta) \end{bmatrix} \quad \text{B.3}$$

B.4 shows rotational matrix from Hub to Blade

$$R_{H2B} = \begin{bmatrix} cos(\theta) * cos(\zeta) & sin(\zeta) & -cos(\zeta) * sin(\theta) \\ sin(\beta) * sin(\theta) - cos(\beta) * cos(\theta) * sin(\zeta) & cos(\beta) * cos(\zeta) & sin(\beta) * cos(\theta) + cos(\beta) * sin(\theta) * sin(\zeta) \\ cos(\beta) * sin(\theta) + sin(\beta) * cos(\theta) * sin(\zeta) & -sin(\beta) * cos(\zeta) & cos(\beta) * cos(\theta) - sin(\beta) * sin(\theta) * sin(\zeta) \end{bmatrix} \quad \text{B.4}$$

B.5 shows rotational matrix from Hub DUST to Hub Simulator

$$R_{D2S} = \begin{bmatrix} 1 & 0 & 0 \\ 0 & -1 & 0 \\ 0 & 0 & -1 \end{bmatrix} \quad \text{B.5}$$

C. Appendix C

In the following section a summary of the table of FSTD validation tests presented in subpart C of [5] is reported. Section 2.c. includes the manoeuvre of interest.

1. **PERFORMANCE**
    a. Engine Assessment
    b. Ground Operations
    c. Take-off
    d. Hover Performance
    e. Vertical Climb Performance
    f. Level Flight Performance and Trimmed Flight Control Position
    g. Climb Performance and Trimmed Flight Control Position
    h. Descent
    i. Auto-rotational Entry
    j. Landing
2. **HANDLING QUALITIES**
    a. Control System Mechanical Characteristics
    b. Low Airspeed Handling Qualities
    c. Longitudinal Handling Qualities
    d. Lateral & Directional Handling Qualities
3. **ATMOSPHERIC MODELS**
4. **MOTION SYSTEM**
    a. Motion Envelope
    b. Frequency Response Band, Hz
    c. Leg Balance
    d. Turn Around
    e. Characteristic vibrations/buffet
    f. Motion Cue Repeatability
5. **VISUAL SYSTEM**
    a. Visual ground segment (VGS)
    b. Display system tests
6. **FSTD SYSTEMS**
    a. Visual, Motion and Cockpit Instrument Response
    b. Sound

D. Appendix D

In this section the Levenberg-Marquardt method (LM) [17] will be presented.

Levenberg-Marquardt is a method that redefines the Fisher information matrix (FIM) to improve the quality of its inverse. The Fisher information matrix is a measure of the amount of information that a variable carry about the estimated parameters. Many methods require the inversion of FIM, that can be nearly singular (ill conditioned), particularly if one of the following conditions occurs:

- Excessive number of unknown parameters.
- Misspecification of the model: it occurs when different parameters induce nearly equal effects on the outputs, or one or more parameters has little or no effect on the outputs.
- Little movement of the outputs results in an apparent misspecification of the model.

The last point is particularly relevant for the case in object, and is the probable reason why this method as been proven the best to identify the system.

LM method augments FIM as in D.1

$$M^{-1} = (M_0 + kA)^{-1} \qquad \text{D.1}$$

Where M_0 is the initial FIM, A is a positive define matrix, typically the identity matrix, and k is a positive nonzero scalar, obtained with an iterative procedure.

List of Figures

List of Tables

List of symbols

Variable	Description	SI unit[1]
β	Flap angle	rad
γ	Local circulation	m^2/s
$[\delta L]$	Inflow perturbation matrix	-
ζ	Lead-lag angle	rad
θ	Pitch angle	rad
λ	Inflow	-
λ_0	Inflow (uniform variation)	-
λ_c	Inflow (longitudinal variation)	-
λ_m	Momentum theory inflow	-
λ_s	Inflow (lateral variation)	-
μ	Stream velocity	-
ν	Generic degree of freedom	/
ρ	Air density	kg/m^3
φ_ν	Phase of a generic degree of freedom	rad
χ	Wake angle	rad
ψ	Azimuth angle	rad
Ω	Rotational speed	-
A_ν	Amplitude of a generic degree of freedom	rad
B	Blade reference frame	/
BY	Helicopter body refence frame	/
C_D	Drag coefficient	-
C_L	Lift coefficient	-
C_l	Roll moment coefficient	-
C_M	Moment coefficient	-
C_m	Pitching moment coefficient	-
C_T	Thrust coefficient	-
D	DUST tilted hub reference frame	/
$F_\#$	Forces on # reference frame	N

[1] The symbol – denotes dimensionless variables, while / denotes unmeasurable entities, or variables with multiple possible meanings.

HF	Hub fixed reference frame	/
HR	Hub rotating reference frame	/
I_θ	Hub tilt angle	rad
K_β	Elastic coefficient of β	Nm/rad
K_ζ	Elastic coefficient of ζ	Nm/rad
$[L]$	Inflow gain matrix	-
$[M]$	Inflow mass matrix	-
$M_\#$	Moments on # reference frame	Nm
N	Number of blades	/
p,q,r	Angular velocity components about fuselage axis	rad/s
R	Rotor radius	m
r	Blade element position	m
$R_{\#2@}$	Rotational matrix from # frame to @ frame	-
$\bar{U}_b$	Velocity of the blade element	m/s
$\bar{V}_b$	Local velocity of the blade element	m/s
$\bar{V}_{in}$	Inflow velocity of the blade element	m/s
w	Downwash	m/s

Acknowledgments

Al termine del mio percorso universitario sono doverosi alcuni ringraziamenti.

In primo luogo ringrazio in mio relatore, il Professor Quaranta, per avermi instradata ed assistita durante il percorso di tirocinio.

Un grazie anche a tutti i colleghi di TXT, in particolare il mio tutor Francesco, Paolo, Matteo e Lapo, per tutto l'aiuto fornitomi e per l'esperienza e la professionalità che hanno scelto di condividere.

Alle amiche dello zoo del Polimi, Chiara, Elena, Erika, Sabrina e Silvia. Abbiamo condiviso questo turbolento volo da sempre, le ansie, le paure, i fallimenti, ma sopratutto le soddisfazioni, le gioie e i festeggiamenti. È stato difficile, ma con voi ne è sempre valsa la pena.

A tutta la mia famiglia.

A mia nonna Imelda, inesauribile fonte di complimenti e cioccolato e, soprattutto, grande esempio di vita.

A mio fratello Samuele Silvio, impareggiabile correttore di bozze, che condivide da sempre tutto con me, incluse le gioie e i dolori dell'ingegneria. Sostegno costante in tutti i momenti di bisogno.

A mamma Susanna e papà Silvio i miei sponsor, soprattutto emotivi. Grazie per aver sempre creduto in me, talmente tanto da sopperire alle mie mancanze. Non smetterò mai di aver bisogno di voi e di ringraziarvi, il merito di questa conclusione è anche vostro.

Infine, il mio pensiero va agli affetti assenti, in paritcolare a mio nonno Pietro Scagliola. La passione per il fare, per imparare e scoprire è una sua eredità. È stato di ispirazione da quando ero piccola e lo vedevo saldare, fino agli ultimi anni, quando si ostinava ad ascoltare le mie infinite spiegazioni sui mezzi aerei. Penso, e spero che sia fiero di me.